AN INVESTIGATION INTO THE EFFECTS OF RUNNING PROPELLERS ON THE STATIC LONGITUDINAL STABILITY OF MULTI-ENGINE TRACTOR-PROPELLER-DRIVEN MONOPLANES

Thesis by

Warren Amster

In Partial Fulfillment of the Requirements

For the Degree of

Aeronautical Engineer

California Institute of Technology

Pasadena, California

1948

ACKNOWLEDGEMENTS

The author wishes to express his sincere appreciation for the advice and guidance of Mr. R. W. Bell and Dr. H. J. Stewart in the preparation of this thesis.

The use of the wind tunnel data presented in this thesis was made possible by the generous cooperation of the Aerodynamics Group of the Consolidated Vultee Aircraft Corporation, San Diego, and the staff of the GALCIT Wind Tunnel.

TABLE OF CONTENTS

I SYNOPSIS

This thesis has three main purposes:

1. To establish an engineering computation procedure for predicting $C_{M(\text{c. g.})}$ as a function of C_L and power conditions for a multi-engine monoplane of conventional configuration with tractor propellers mounted on and forward of the wing from a given curve of C_M as a function of C_L for the power-off condition.

2. To recommend aircraft configurations which will minimize the destabilizing effect of power.

3. To provide a physical explanation of the effect of power on stability.

Calculated C_M vs. C_L curves are compared with "matched-power" wind tunnel model test results. The agreement is good for all-right-hand rotation of propellers but unsatisfactory for other rotation modes.

II INTRODUCTION

Some recent high performance propeller-driven aircraft have shown very marked effects of running propellers on static longitudinal stability. Reports from this country and from England, Germany and France mention the phenomenon. Although the effect varies considerably in magnitude among different aircraft, it is almost always destabilizing. There is a considerable body of literature reporting on wind-tunnel investigations into this and contributory phenomena. It is the purpose of this report to compile the available information that seems pertinent to the subject and arrange it into a simple computation procedure to predict stability of monoplane tractor-propeller-driven aircraft.

The data upon which this report is based were taken by a great many different investigators with greatly varying experimental equipment and techniques. Whenever possible the results of several investigators have been checked against each other in order to verify any theory which attempted to describe their experimental results. In general the data correlated quite well. In several cases some rather broad assumptions were necessary in order to obtain values for quantities which were necessary for computation purposes and which were either not mentioned in the literature or not measured by the investigators. An example is model propeller characteristics which were obtained largely from propeller charts which were not necessarily those for the propellers used in the tests. Errors introduced by such assumptions were minimized by averaging the results of as many different tests as possible.

The method of presentation is planned to help give a physical reason for separate effects and then combine all separate effects into a complete calculation procedure. In Sec. III the separate forces and

moments are discussed and means of calculating them presented. Sec. IV presents the calculated results for five airplanes for which wind tunnel data were available. The calculations are compared with experimental results and the accuracy of the different phases of the calculations discussed. Sec. V gives a recommended tabular computation procedure which incorporates the portions of the calculations which agree consistently with experiment. C_L and C_M are calculated as functions of α.

In several reports cited as references, stability curves show characteristics for which the investigator who noted them had no explanation. These effects will be discussed in connection with the particular part of the calculations that the affect. They are seldom of primary importance but they sometimes have a noticeable effect on stability and they cannot be predicted by the calculations employed in this report. The complicated interaction and interference associated with flow of a slipstream over parts of an airplane could logically be expected to result in some incalculable forces and moments. However these unexplained effects are definitely associated with particular aircraft and are shown not to be typical of any general configuration. It is assumed that they are the result of nacelle shape, fillets, spanwise flow, separation or some other unknown characteristic of particular aircraft. Wind tunnel tests appear to be the only way of predicting such effects.

Scope

Configuration: The calculation method of this report is applicable to the following type of aircraft:

1. A conventional monoplane with tractor propellers on nacelles mounted on the wing. The airplane may have any even number of propellers. The axis of propeller rotation must pass reasonably close to the wing chord line.

The analysis is intended to be applicable to the following special

cases. The accuracy of the calculations for each case as compared to experimental data is discussed in Sec. IV.

1. All propellers turning in the same direction, power symmetrical.
2. Unsymmetrical power.
3. Opposite rotating propellers with blades moving up in the center.
4. Tailless aircraft with tractor propellers.
5. Any number of propellers feathered.

The following cases may not be treated by this method:

1. Extended flaps, spoilers, dive brakes, fuselage brakes, bomb bay doors, or landing gear and externally attached bombs, torpedoes, armament or fuel tanks whenever any of these objects interfere with the flow in the slipstream in such a way as to disturb the flow past the wing or tail of the airplane. Whether this disturbance will invalidate the analysis is left to the discretion of the designer.

Power Conditions: Three distinct power conditions will be considered.

1. Constant thrust wind-tunnel power-model polar. For this condition the RPM of the model propeller is held constant through out the test range of angle of attack.
2. "Matched Power" wind-tunnel power model polar. The RPM of the model propellers is varied for constant blade setting so that T_c' of the model equals T_c' for the simulated full-scale airplane flying at equivalent C_L.
3. Full scale airplane in flight. The airplane is assumed to fly from stall to maximum level flight speed with constant power output and constant propeller RPM.

Power conditions 2. and 3. can theoretically be treated as equivalent for all phenomena dependent on T_c' if scale and compressibility effects are neglected. Although T_c' is the same for these two cases, the conditions of constant blade angle for the model, and constant propeller RPM for the full scale airplane, introduce differences in C_p and J. These differences are usually small as shown in Ref. (1). However under certain circumstances it might be necessary to consider the cases separately. For the purposes of this report power conditions 2. and 3. will be assumed to be equivalent.

The effects of Reynolds Number and Mach Number on the phenomena described in this report is not known.

Only conditions of steady state flight will be considered.

Notation

Dimensions. Throughout this report all equations are adjusted to use data with the following dimensions:

Lengths	-	Feet
Areas	-	Square Feet
Velocities	-	Feet per Second
Forces	-	Pounds
Pressures	-	Pounds per Square Foot
Moments	-	Pound-feet
Power	-	Foot Pounds per Second
Angles	-	Radians
Rotational Speeds	-	Revolutions per Second

Coordinate System. Fig. (1) shows the conventions for dimensions and angles used in this report.

Dimensions denoted by $x_{(\ )}$, $y_{(\ )}$ and $z_{(\ )}$ refer to a Cartesian coordinate system with its origin at the center of gravity of the airplane. The positive $x_{(\ )}$ direction is aft in any geometrically

convenient direction (ie. wing chord line, fuselage reference line) The positive $y_{(\ )}$ direction is up normal to the x axis. All $z_{(\ )}$ dimensions are positive and are measured normal to the plane of symmetry. Subscripts identify dimensions. All dimensions shown in Fig. (1) are positive except x_p. Dimensions measured in other directions are given symbols other than $x_{(\ )}$, $y_{(\ )}$ and $z_{(\ )}$.

Vertical angles denoted by $i_{(\ )}$ are referred to the $x_{(\ )}$ axis. They are positive when they are as shown in Fig. (1). The angle of attack, α, is the angle between the x axis and the direction of relative wind, positive as shown. Horizontal angles denoted by $\theta_{(\ )}$ are measured with respect to the plane of symmetry and are positive as shown in Fig. (1). Subscripts identify angles.

Forces are referred to any direction in keeping with their physical nature. As an example; lift is positive up, referred to a direction normal to the relative wind; thrust is positive forward, referred to the thrust axis.

All pitching moments are taken about the center of gravity of the airplane, positive when they tend to raise the nose.

The right-hand side of the airplane is to an observer's right when he is standing behind the tail of the airplane, facing toward it and the airplane is parked on its landing gear.

A propeller has a right-hand rotation when the upper blades are moving to the airplane's right.

Propellers are numbered from left to right. The subscripts on A_p, B_p, T_c' and R identify which propeller they apply to.

Symbols

Symbol	Description	Reference
A	Propeller Coefficient.	Fig. (2)
A_{p_i}	Distance from Propeller Plane to Center of Gravity, measured parallel to thrust axis, positive for tractor propellers. Subscript identifies propeller.	
a	Radial Velocity in Slipstream at propeller disc.	
a'	Radial Velocity in Slipstream far downstream from propeller.	
a_o	Slope of Lift Curve for Wing Airfoil Section in Infinite Aspect Ratio Wing.	
a_{o_t}	Slope of Stabilizer Airfoil Section for Infinite Aspect Ratio.	
a_t	Slope of Normal Force Coefficient Curve for Stabilizer.	$dCn_t/d\alpha$
B	Propeller Coefficient	Fig. (2)
B_{p_i}	Distance from Thrust Axis to Center of Gravity, measured normal to thrust axis, positive for thrust axis above C.G. Subscript identifies Propeller.	
b	Propeller Blade Chord at r = 0.7D/2	
C	Propeller Factor.	Equation (10)
C_L	Lift Coefficient for Complete Airplane, power-on.	$C_L = 2L/\rho V_o^2 S$
ΔC_L	Lift Coefficient Increment due to Slipstream over Wing.	Equation (12)
C_{L_o}	Lift Coefficient for Complete Airplane power-off.	
C_M	Pitching Moment of Complete Airplane, power-on.	$C_M = 2M/\rho V_o^2 Sc$
C_{M_o}	C_M, Tail Off, power-off.	
C_{N_t}	Normal Force Coefficient of Stabilizer.	$C_{N_t} = 2L_t/\rho V_o^2 S_t$ Equation (15)
C_p	Power Coefficient.	$C_p = P/\rho N^3 D$

Symbol	Description	Reference
C_T	Thrust Coefficient.	$C_T = T/\rho N^2 D^4$
c	Mean Aerodynamic Chord.	
D	Propeller Diameter.	
E	Number of Propellers Operating.	
e	Elevator Deflection Angle, positive for trailing edge down.	
e_v	Slipstream Deflection Angle.	Equation (10)
F	Slipstream Deflection Factor	Equation (10)
g	Axial Velocity at Propeller Disc	
g'	Axial Velocity in Slipstream far downstream from Propeller	
G	Fraction of Stabilizer Area in Slipstream.	Fig. (6)
H	Slipstream Rotation Factor.	Fig. (4)
h	Dimensionless Slipstream Coordinate.	Equation (14)
i_{p_i}	Angle between Thrust Axis and x Axis. Subscript identifies propeller.	Fig. (1)
i_t	Angle between Stabilizer Zero-Lift Line at e = 0 and x Axis.	Fig. (1)
Δi_t	Change in Angle of Stabilizer Zero-Lift Line due to Elevator Deflection.	$\Delta i_t = eK$
J	Propeller Advance-Diameter Ratio.	$J = V_o/ND$
j	Chord of Wing in Vertical Plane through Thrust Axis. Use average value for four and six engine aircraft.	
K	Elevator Effectiveness Factor.	$K = \Delta i_t/e$
k	Downwash Factor.	
L	Lift Force on Airplane power-on measured normal to relative wind.	
L_T	Normal Force on Stabilizer.	
M	Pitching Moment of Airplane, power-on, taken about center of gravity, positive when moment tends to raise nose of airplane.	
m	Downwash Factor.	

Symbol	Description	Reference
N	Propeller Rotational Speed.	
n	Number of Blades per Propeller.	
P	Power per Engine.	
Q	Propeller Solidity at r = 0.7D/2.	Equation (4)
q	Local Dynamic Pressure.	$q = \rho V^2/2$
q_o	Dynamic Pressure of Relative Wind.	$q_o = \rho V_o^2/2$
R_i	Propeller Normal Force Coefficient Derivative. Subscript identifies propeller.	Equation (4)
r	Radial Coordinate of Propeller	
S	Wing Area.	
S_t	Stabilizer Area.	
s	Slipstream Velocity Factor.	Equation (8)
T	Thrust Force, positive foreward, parallel to thrust axis, for one propeller.	
T_c	Thrust Coefficient.	$T_c = T/\rho V_o^2 D^2$
T'_{c_i}	Thrust Coefficient. Subscript Identifies propeller.	$T'_c = 2T/\rho V_o^2 S$
U	Slipstream Factor.	Fig. (6)
u	Slipstream Velocity Increase Factor	Equation (7)
V	Local Air Velocity.	
V_o	Velocity of Aircraft.	
v	Dimensionless Slipstream Coordinate.	Equation (13)
W	Total Velocity behind Propeller.	
W'	Total Velocity far downstream from propeller.	
w	Angle of Downwash from Wing at Stabilizer.	
x_p	Abscissa of Inboard Propeller Hub.	Fig. (1)
x_t	Abscissa of Elevator Hinge Line.	Fig. (1)
x_w	Abscissa of Wing Center of Pressure.	Fig. (1)
y_p	Ordinate of Inboard Propeller Hub.	Fig. (1)

Symbol	Description	Reference
y_t	Ordinate of Stabilizer Center of Pressure.	Fig. (1)
y_w	Ordinate of Wing Center of Pressure	Fig. (1)
z_p	Distance from Propeller Hub to Plane of Symmetry, measured normal to plane of symmetry, always positive.	Fig. (1)
z_t	Stabilizer Semispan.	Fig. (1)
α	Angle of Attack, measured between some reference direction and the relative wind, positive when the nose is raised.	
γ	Helix Angle of Flow in Slipstream at Propeller Disc.	
γ'	Helix Angle of Flow in Slipstream far Downstream from Propeller.	
η_t	"Stabilizer Efficiency Factor," power-off	
θ_p	Horizontal Angle between Thrust Axis and Plane of Symmetry, positive as shown in Fig. (1).	Fig. (1)
λ	Slipstream Inclination Factor.	
ρ	Air Density, in slugs/cubic foot.	
ψ	Angle of Downwash due to rotation in Slipstream.	
ψ_o	Function expressing variation of angle of Downwash due to rotation in Slipstream in terms of location in Slipstream.	

III EFFECT OF POWER ON AIR LOADS ACTING ON AIRCRAFT

General Remarks.

The most common means of representing static longitudinal stability is a plot of $C_{M_{(c.g.)}}$ vs. C_L for any desired power condition. Stability is then measured by $-dC_M/dC_L$. In the simple theory without power the plot of C_M vs. C_L is a straight line if the center of gravity of the airplane is on the chord line. For this theory $-dC_M/dC_L$ can be calculated without calculating C_M first. The stability can also be calculated for the case where the center of gravity is above or below the chord line. However this configuration introduces curvature into the C_M vs. C_L curve and the trim condition is important so that C_M must be calculated and then equated to zero.

The introduction of running propellers into the configuration has a great many effects on C_L, dC_L/d , C_M and dC_M/dC_L. These effects depend on such variables as J, T_c', tail length, location of thrust axis, and propeller characteristics. By making some very approximate assumptions it is possible to calculate $-dC_M/dC_L$ for trim at a given power condition. However there are many conditions under which these assumptions lead to extremely erroneous results. For this reason it was decided to calculate C_M as a function of C_L, power, and elevator deflection and use the graphical slope of the C_M vs. C_L curve to obtain $-dC_M/dC_L$. This is the form in which wind tunnel data are obtained and the correlation of the calculated and wind tunnel data is then quite simple.

Propellers.

Thrust. For any stability calculations it will be assumed that a standard performance analysis has already been carried out for the airplane so that "power available" curves are at the disposal of the designer. From the "power available" curves and the condition of

steady flight it is quite simple to calculate curves of power and thrust coefficients and advance ratio as functions of C_L for each propeller.

The propeller thrust coefficient which is analogous to C_L for static equilibrium calculations is T_c'. Ref. (2) states that the thrust of a propeller is not affected by small angles of pitch with respect to the relative wind. It will be assumed here that T_c' is not affected by any angle of pitch encountered in flight.

T_c' may be calculated as a function of C_L as follows:

① $$T_c' = \frac{2T}{\rho V_o^2 D^2}$$

② Lift Component of T_c': $= ET_c' \sin(\alpha + i_p) = ET_c'(\alpha + i_p)$

③ Pitching Moment Contribution of T_c': $= \frac{-ET_c'B_p}{c}$

Propeller Normal Force. A running propeller whose thrust axis is at an angle to the relative wind experiences a force in the plane of rotation. This force is a function of the angle of inclination, thrust loading, thrust grading and number of blades.

Ref. (3) gives a method of computing the force for three representative blade planforms. The same data are used in Ref. (4) with a slightly different method. It appears that the method of Ref. (3) is in somewhat better agreement with experiment and it is used here.

The propeller side force coefficient analagous to C_L for static equilibrium calculations is $R(\alpha + i_p)$.

R may be calculated as a function of C_L as follows:

④ $$R = (AQ + \frac{BC_T}{10})\frac{D^2}{S} \qquad \text{where} \qquad Q = \frac{nb}{0.7\pi D}$$

A and B from Fig. (2)

⑤ Lift Component of Propeller Normal Force:

$$= R(\alpha + i_p)\cos(\alpha + i_p) \doteq R(\alpha + i_p)$$

⑥ Moment Contribution of Propeller Normal Force:

$$= \frac{R(\alpha + i_p)A_p}{c}$$

A propeller at an angle to the relative wind also experiences a destabilizing moment about the propeller hub. Ref. (1) states that it is insignificant when compared with other pitching moments of the airplane. It will be neglected in this report.

Flow in the Slipstream.

Velocity Increase. The momentum theory for propellers treats the propeller as a disc with a pressure difference across it. The resulting flow is a contracting region of increasing velocity downstream of the propeller. Theoretically the slipstream velocity approaches a fixed value far downstream and the slipstream continues indefinitely. Actually viscous mixing at the slipstream boundary causes the edges of the slipstream to become indistinct and the flow tends to return to the undisturbed velocity very far downstream. Wake surveys in Refs. (5, 6, 7, 8) indicate that the magnitude of the velocity increase in the slipstream approximates the theoretical values in the region of the wing and stabilizer of a conventional airplane. The size and shape of the slipstream and the approximations to be used in this report will be discussed in the sections dealing with forces arising from the presence of the slipstream. Again it is assumed that tilting of the propeller axis does not affect the thrust of the propeller or the increase in velocity in the slipstream.

This velocity increase is most usefully expressed as the ratio of $V^2_{(slipstream)}$ to V_o^2. This ratio is also the ratio of the dynamic pressures q/q_o, which is of the most fundamental importance here.

Dynamic pressure ratios in the slipstream are calculated as functions of C_L as follows:

⑦ Dynamic Pressure Ratio at Propeller Disc:

$$q/q_o = (1 + u)^2 \qquad \text{where } u = \frac{1}{2}\left[-1 + \sqrt{1 + \frac{8T_c}{\pi}}\right]$$

⑧ Dynamic Pressure Ratio at Wing Center of Pressure:
(Note: This expression is given in Ref. (9).)

$$q/q_o = (1 + s)^2 \qquad \text{where} \qquad s = u\left[1 + \frac{(x_w - x_p)}{\sqrt{\frac{D^2}{4} + (x_w - x_p)^2}}\right]$$

⑨ Dynamic Pressure Ratio at Stabilizer Center of Pressure:

$$q/q_o = (1 + 2u)^2 = 1 + \frac{8T_c}{\pi}$$

Deflection of Slipstream. A propeller with its thrust axis inclined to the relative wind experiences two forces normal to the relative wind, both in the same direction. One force is the thrust component normal to the relative wind, the other force is the normal force in the propeller plane. These forces arise from a change of momentum of the air normal to the relative wind. The effect of this momentum change in the slipstream is a deflection toward the inclined thrust axis.

Ref. (2) gives an expression for the ratio of the inclination of the slipstream to the inclination of the thrust axis for small angles of deflection. Experimental data in Refs. (6, 7, 10, 11, 12, 13) indicate that this expression gives sufficiently accurate results for all angles encountered in flight. The angle of inclination of the slipstream to the relative wind is $e_v = F(\alpha + i_p)$. Ref. (2) also gives the ratio of the inclination of the slipstream at the propeller disc to the inclination downstream in the wake as $u(1 + 2u)/2u(1 + u)$ or approximately 1/2 for small u. It will be assumed that the value of the inclination of the slipstream is $e_v/2$ at the propeller and

increases to the full value in the vicinity of the stabilizer. There is some indication that viscous mixing at the slipstream boundary and the "inclined cyclinder" effect of Ref. (9) tend to decrease the theoretical value of e_v as the slipstream progresses downstream. This possibility and also the uncertainty in the calculated value will be investigated by introducing an undetermined coefficient λ multiplying e_v anywhere that errors in its determination could lead to first order errors. The coefficient will then be determined by experimental data.

e_v may be calculated as a function of C_L as follows:

(10) $e_v = F(\alpha + i_p)$ where $F = \dfrac{2u(1+u)\left[1 + (C/T_c)\right]}{(1+2u)\left\{1 + u\left[1 + (C/T_c)\right]\right\}}$

F is plotted as a function of T_c and C in Fig. (3). This plot should be used for design purposes.

$$u = \frac{1}{2}\left[-1 + \sqrt{1 + \frac{8T_c}{\pi}}\right]$$

$$C = \frac{RS}{2D^2}$$

R from Equation (4)

Note: The expression in Ref. (9) uses values for C which are calculated differently than is done here. The physical significance of the two factors is the same and the one given here is used because it is simpler to calculate and seems to be more accurate.

Rotation in the Slipstream. The torque of a running propeller causes rotational velocity components of flow in the slipstream. The radial distribution of rotation immediately behind the propeller depends on the torque grading of the propeller. Farther downstream the effects of viscosity modify the rotational velocities which are typical of a

particular propeller and produce a pattern which tends to be the same for all propellers. Wake surveys behind wing-propeller combinations show this effect clearly. Plots of velocity distribution and/or downwash angle in a plane normal to the free stream direction in the position normally occupied by an airplane stabilizer were found in Refs. (6, 7, 8, 12, 14, 15, 16, 17). These surveys show that several propeller diameters downstream of a wing-propeller combination the slipstream takes on a characteristic shape, axial velocity distribution and rotational velocity distribution.

In this report the method of predicting the magnitude and distribution of the rotational velocities in the slipstream is to derive a parameter upon which the magnitude of the helix angle of flow due to rotational velocities depends and then reduce experimental data to a typical angular distribution in the slipstream in terms of that parameter. Data from the references cited above indicate that this procedure is generally reliable for predicting the downwash at a stabilizer due to rotation in the flow behind a propeller.

Parameter Governing Slipstream Rotation as a Function of C_L:

Ref. (2) gives an expression for the radial gradient of power-coefficient of a propeller acting in an incompressible fluid (in the notation of this report):

$$\frac{dC_p}{dr} = \frac{4\pi^2 r^2 g a}{D^5 N^2}$$

where: r = radial coordinate of propeller

g = axial velocity at propeller disc for radius r.

a = rotational velocity in slipstream at propeller disc for radius r.

Considering the components of velocity in the slipstream:

γ = helix angle of flow due to rotational velocity immediately behind propeller.

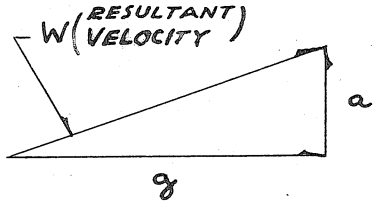

$$a/W = \sin\gamma \;;\quad g/W = \cos\gamma \;;\quad ag/W^2 = \sin\gamma\cos\gamma = \frac{\sin 2\gamma}{2}$$

Substituting into the expression for dC_p/dr:

$$\frac{dC_p}{dr} = \frac{2\pi^2 r^2 W^2 \sin 2\gamma}{D^5 N^2}$$ where: W and γ are both functions of r.

It is now assumed that streamlines which pass through the propeller form concentric circular cylinders which have a reduced radius downstream but maintain their identity and relative geometrical position. Primed symbols are for conditions far downstream from the propeller. The following sketch illustrates the assumed flow:

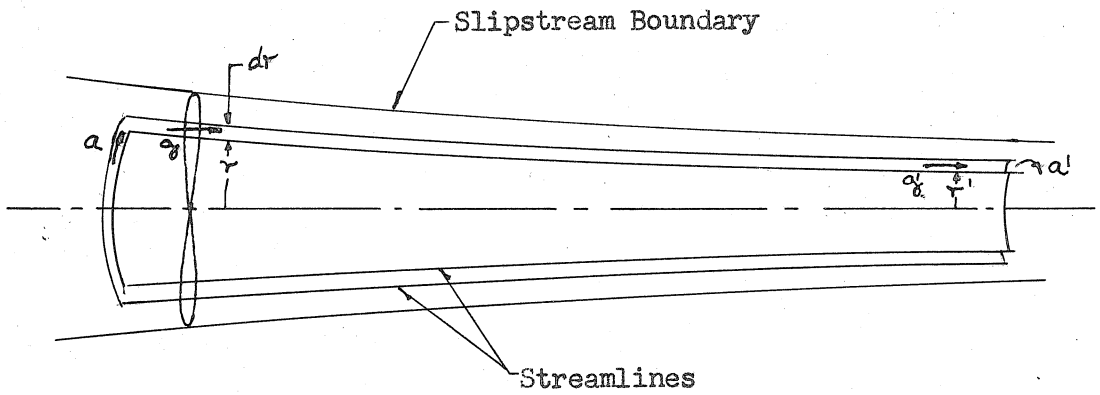

Making the assumption that g and g' have the same functional dependence on r/D and r'/D' respectively, continuity of flow between streamlines a distance dr apart at the propeller disc gives:

$$g'/g = r^2/r'^2$$

Conservation of angular momentum gives:

$$r^2/r'^2 = a'/a$$

Considering flow far downstream from the propeller:

$$\frac{W'^2 \sin 2\gamma'}{2} = g'a'$$
$$= ga(g'a'/ga)$$
$$= \frac{W^2 \sin 2\gamma}{2}(g'/g)^2$$

Substituting:

$$\frac{dC_p}{dr} = \frac{2u^2r^2W'^2\sin 2\gamma'}{D^5N^2}(g/g')^2$$

This is an expression relating the power coefficient grading of a propeller to the angle of flow due to rotation far downstream from the propeller.

In general W', γ', g and g' will be functions of r so this expresssion is not directly integrable. However in order to derive a parameter upon which the downwash due to rotation will depend, these variables will be replaced by mean values outside the integral sign. This is possible because W'^2, $\sin 2\gamma'$, g^2 and $1/g'^2$ all satisfy the conditions of the Theorem of the Mean as given in Ref. (18).

$$C_p = \int_0^{D/2} dC_p = \frac{2\pi^2}{D^5N^2}\int_0^{D/2} \frac{W'^2\sin 2\gamma' g^2 r^2\, dr}{g'^2}$$

$$= \frac{2\pi^2\overline{W'^2\sin 2\gamma'}\ \overline{g^2}}{D^5N^2\overline{g'^2}}\int_0^{D/2} r^2dr$$

$$= \frac{\pi^2W'^2\overline{\sin 2\gamma'}}{12\,D^2N^2}\ \frac{\overline{g^2}}{\overline{g'^2}}$$

Assuming that γ' is small and taking mean values for W'^2, g and g' from the simple momentum theory:

$$\overline{W'} = V_o(1 + 2u) \qquad \text{where;} \quad u = \frac{1}{2}\left(\sqrt{1 + 8T_c/\pi} - 1\right)$$

$$\overline{g} = V_o(1 + u)$$

$$\overline{g'} = V_o(1 + 2u)$$

$$C_p = \frac{\pi^2\gamma' V_o^2(1 + u)^2}{6D^2N^2}$$

Giving:

$$\overline{\gamma'} = \frac{6C_p}{\pi^2J^2(1 + u)^2}$$

Finally assuming that u is small compared to 1 (lightly loaded propeller):

$$\overline{\gamma'} = \frac{6C_p}{\pi^2 J^2(1 + 4T_c/\pi)}$$

This analysis indicates that the mean helix angle of rotation in the slipstream far downstream from the propeller is proportional to $C_p/J^2(1 + 4T_c/\pi)$. The vertical component of this rotation angle will give the predominant effect on the stability because it contributes to the downwash at the stabilizer. Downwash surveys behind wing-propeller combinations in Ref. (7, 8, 12, 14, 15) were analyzed by subtracting the portion of the downwash which was constant across the slipstream leaving only the components due directly to rotation. These were put in the form:

(11) $$\psi = \psi_o \, C_p/J^2(1 + 4T_c/\pi)$$

where: ψ = angle of downwash due to rotation as a function of the location in the slipstream and of the propeller operating conditions.

ψ_o = function describing the distribution of ψ in the slipstream independent of propeller operating conditions.

Contours of ψ_o throughout the slipstream from Refs. (7, 8, 12, 14, 15) were compared and good agreement in both magnitude and distribution was found. A plot of ψ_o which represents a mean of these curves is used for calculation purposes. This plot is shown in Fig. (4a) in coordinates reduced to dimensionless form in terms of the propeller diameter. To find ψ at a particular location in the slipstream (location with respect to the center of the slipstream at the stabilizer hinge line), multiply the value of ψ_o at that location by the parameter $C_p/J^2(1 + 4T_c/\pi)$ for the operating conditions of the propeller.

The use of this development in predicting the effects of rotation

in the slipstream will be presented under Stabilizer Lift and Pitching Moment on page (30).

Rotation in the slipstream is one of the flow phenomena which is not matched when a flying airplane with constant-speed propellers is simulated in a wind tunnel by a model with fixed-pitch propellers. No data have been found which can give some indication of actual experimental variations for these cases. It appears reasonable to neglect these differences until the accuracy of the whole computation procedure is established and then examine them as compared to the overall accuracy.

Flow Over Wing and Nacelle:

Lift Increment. The region of increased velocity over the wing behind a propeller results in an increase in lift over that portion of the wing. Spanwise and chordwise lift distribution surveys of Ref. (7) show that the rotational components of velocity in the slipstream have a first order effect on spanwise lift distribution. However the total lift increment can be calculated without regard to rotation provided the propeller is far enough ahead of the wing leading edge. This is the situation for the usual nacelle arrangement of modern aircraft as indicated by data from Ref. (9) where the effect was investigated.

The lift increment is calculated as ΔC_L and added to the lift of the airplane without power. Ref. (9) gives a method for finding this lift increment involving determination of the lift distribution and a parameter which is a function of the aspect ratio of the portion of the wing in the slipstream.

A considerable simplification in the calculations appears to be possible by using a modification of the method of Ref. (9). This modification uses the total lift coefficient to calculate ΔC_L. The expression given below predicts ΔC_L accurately for the five air-

airplanes for which data were available. It should be noted here that experimental verification of the following equation has been obtained only for two and four engine airplanes with symmetrical power all of which were tested in the same wind tunnel.

ΔC_L due to power may be calculated as follows:

(12) $$\Delta C_L = \frac{EDjs}{S}\left(C_{L_o} - 0.6a_o e_v\right)$$

where s from Equation (8)

e_v from Equation (10)

Note: s and e_v are indirect functions of C_L. However C_L must be calculated in order to find C_L. This requires a sucessive approximation process which will be discussed on page (34).

Other Effects. Experiments in Refs. (6, 7, 12, 13,) indicate that the increment of C_{M_o} due to a slipstream passing over a wing is negligible.

The flow near nacelles is of such a random nature that no calculation of its effects can be made. The usual procedure of estimating power-off nacelle contribution to pitching moment is all that can be recommended. Unfortunately pronounced interference effects can occur which are of some unknown nature. Ref. (19) cites several cases of noticeable effects on the pitching moment of different propeller rotation modes. The effects were noted in wind tunnel tests and no information on verification by flight tests is available. No instance of any such interference on a wing without nacelles has been noted.

Flow Over Stabilizer.

The flow in the vicinity of the horizontal stabilizer of a conventional tractor multi-engine monoplane consists of a region of wing downwash surrounding well defined, characteristically shaped slipstreams. The distortion from a circular shape of the slipstreams results from

the interaction of the rotational components of the slipstream and the wing. In the region where the slipstream flows past the wing the vertical components of the rotation are blocked while the horizontal components cause horizontal translations of the upper and lower portions in opposite directions. Downstream of the wing these two sheared portions do not reunite but tend to progress downstream rotating slightly and giving a shape to the slipstream such as is shown in Fig. (4b). Since the rotation in the slipstream causes the shearing, it is to be expected that the shape of the slipstream is a function of the rotational components in it. This is verified at least qualitatively by all the data available. Assigning a definite shape to the slipstream is also difficult because of the indistinct border between the region of increased velocity and the undisturbed flow. The size and shape of the slipstream behind a wing-propeller combination are defined in this report based on the following assumptions:

1. For a given dynamic pressure survey in a slipstream, the flow is idealized into a region of increased velocity as given by the momentum theory. The following sketch shows a typical plot of dynamic pressure ratio in a slipstream from Ref. (5) and the idealized slipstream which will be assumed. The idealized slipstream boundary is defined so that the area under the wake survey curve is the same as the area under the idealized curve. When generalized to two dimensions, this method of definition of the slipstream boundary permits giving a specific shape to the slipstream which is determined by experiment.

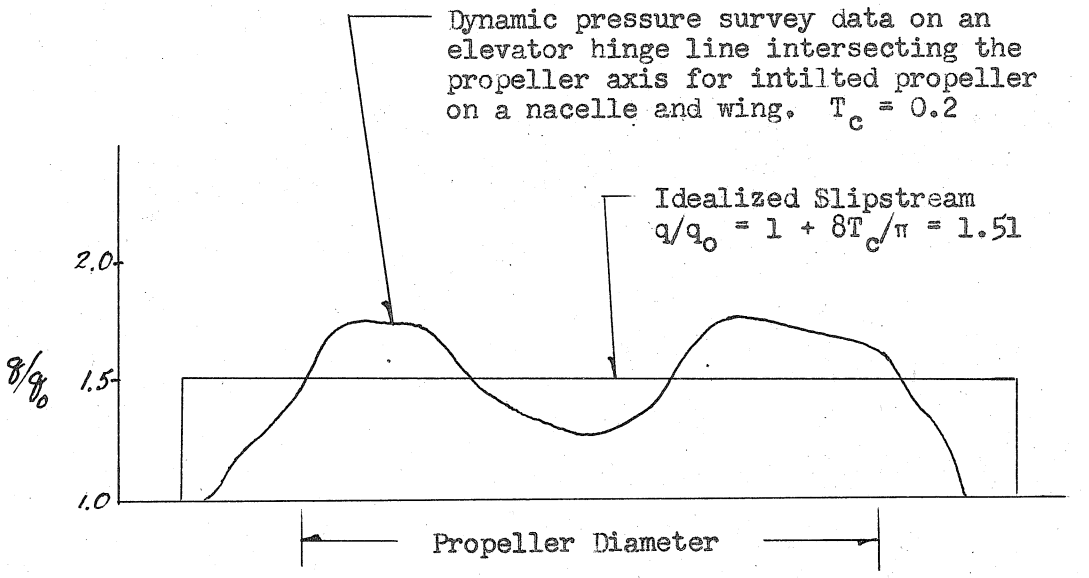

2. For different power conditions the defined shape of a slipstream varies due to different contraction and rotation. Typical variations are shown in the following sketch from wake surveys in Ref. (5).

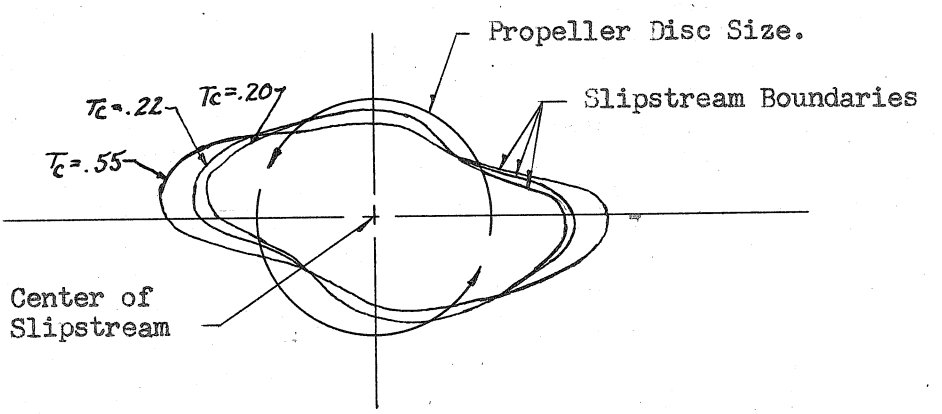

Computing a different shape for a slipstream for each different power condition leads to complications which do not seem justified at this stage of the analysis. At ordinary propeller thrust loadings the shape of a slipstream does not vary greatly with changing propeller operating conditions. Data from Refs. (5, 6, 7, 8) verify this effect for values of thrust loadings which are typical of wind tunnel model tests. These data were used to compute an average shape which is typical of slipstreams of propellers operating at T_c near 0.25.

Fig. (4b) shows this shape. It will be used for all power conditions in the analysis of this report. The slipstream shape chosen will be most accurate for matched power wind tunnel tests in the range of lift coefficients just below the stall where the effects of running propellers on stability are most pronounced.

The simplifying assumptions concerning the nature of the slipstream near the stabilizer would clearly divide the flow field into two distinct regions if it were not for rotation. Outside the slipstream, which is defined by Fig. (4b), the flow would be the same as though the airplane were unpowered except for a slight increase in wing downwash due to the increase in C_L. Inside the slipstream there would be the same downwash angle from the wing as outside, the velocity would be increased by a factor $1 + 8T_c/\pi$ and there would be an additional downwash from the inclination of the slipstream. Unfortunately the rotation field extends outside the slipstream as shown by a comparison of Fig. (4a) and Fig. (4b). The extension of rotational velocities outside the assumed slipstream boundary means that it is impossible to make the assumption that the effect of the presence of the slipstream is felt only by parts of the airplane which actually enter the slipstream.

Because of the behavior of the rotational velocities it will be necessary to make somewhat different assumptions than those outlined above when computing their contribution to the forces acting on the stabilizer of an airplane. The simple assumption of a slipstream with definite shape and increased velocity will be used in computing all effects except rotation. For the rotation analysis somewhat modified assumptions will be used and they will be discussed in the section on rotation.

Wing Downwash. For an airplane without propellers the downwash

at the tail usually varies across the span of the stabilizer because of the disturbance caused by the fuselage or nacelles. The mean downwash is most conveniently expressed in terms of the stabilizer angle at which the stabilizer normal force is zero. Based on such a definition, the downwash angle can be expressed in the form:

$$w = m + kC_L$$

For elliptical lift distribution over the wing and no fuselage or nacelles, m is theoretically zero. Most airplanes show some finite value of m, sometimes as large as 2^o.

In this report it will be assumed that the downwash has the form shown above and that m and k are constants. The value of k can be estimated from three dimensional wing theory. In general m can be found only by tests.

It should be noted here that for a fixed angle of attack, C_L varies with power due to propeller forces and the slipstream passing the wing. This added lift must appear as downwash and the largest portion of it comes from the increased lift of the wing. Calculating w in terms of C_L will give this increased downwash with power-on at a fixed angle of attack.

Location of the Slipstream. For the purposes of this report the vertical location of the slipstream at the stabilizer will be determined based on the following assumptions.

1. The propeller causes the slipstream to have an inclination to the relative wind of $e_v/2$ at the propeller and e_v far downstream. Since the expression for the variation between these values is not known accurately, it will be assumed that the deflection of the slipstream is as though it were all inclined at an angle $0.75e_v$ to the relative wind.
2. The slipstream is assumed to be far enough from the fuselage so that the effects which cause downwash at $C_L = 0$ do not

contribute to the wing downwash in the slipstream. The downwash from the wing is then kC_L in the vicinity of the stabilizer. At the wing this angle is $kC_L/2$ in accordance with three dimensional wing theory. The deflection of the slipstream due to the wing downwash will be assumed to be the same as though it were $0.75kC_L$ from the wing to the stabilizer. The induced flow field from the bound vorticity of the wing is assumed to have no effect on the displacement of the slipstream.

The following sketch illustrates the means of locating the vertical position of the slipstream.

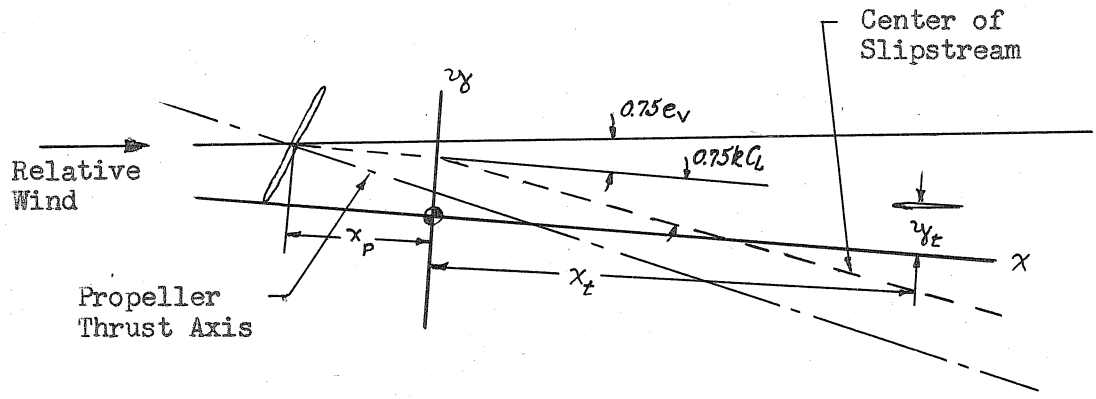

Rather than find the location of the center of the slipstream directly, it will be found in terms of a cartesian coordinate system in the y, z plane at $x = x_t$. These coordinates give the location of the tip of the stabilizer with respect to the center of the slipstream. Such coordinates, when made dimensionless by dividing by the propeller diameter, will permit easy determination of the fraction of the stabilizer which is in the slipstream. The dimensionless coordinates are v and h.

v and h are calculated as functions of C_L as follows:

The distance below the propeller hub of the slipstream center at the wing center of pressure is:

$$(x_w - x_p)\tan(0.75e_v)$$

At the stabilizer this distance is:

$$(x_w - x_p)\tan(0.75e_v) + (x_t - x_w)\tan(0.75e_v + 0.75kC_L)$$

The distance of the stabilizer below the propeller hub is:

$$(x_t - x_p)\tan\alpha - (y_t - y_p)$$

Subtracting and assuming all angles small enough so that tangents can be replaced by angles:

$$(x_w - x_p)0.75e_v + (x_t - x_w)(0.75e_v + 0.75kC_L) - (x_t - x_p)\alpha + (y_t - y_p)$$

Collecting terms and dividing by D:

(13) $$v = \frac{(y_t - y_p) + (x_t - x_w)0.75kC_L - (x_t - x_p)(\alpha - 0.75e_v)}{D}$$

Similiarly:

(14) $$h = \frac{(z_p - z_t) - F\Theta_p(x_t - x_p)}{D}$$

where C_L Lift coefficient power-on.

e_v from Equation (10)

F from Equation (10)

The meaning of v and h is illustrated by the following sketch:

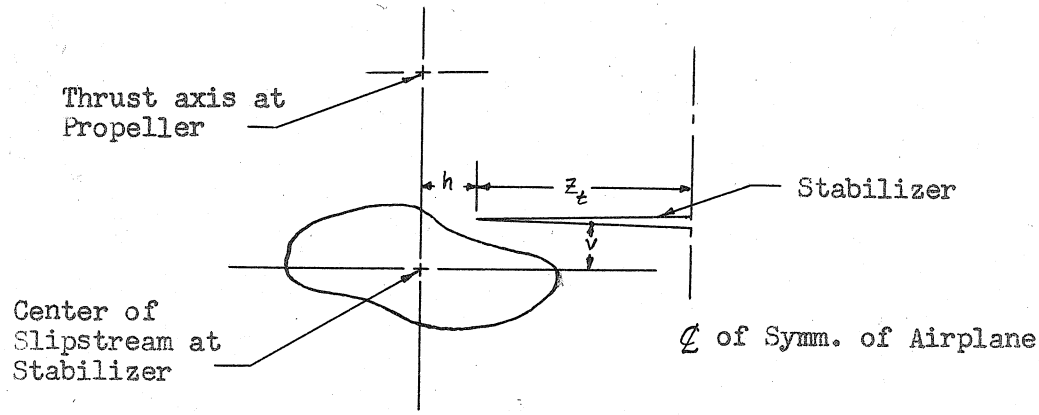

Fraction of Stabilizer in Slipstream. Once the coordinates v and h have been calculated and the shape of the slipstream established, the portion of the stabilizer in the slipstream can be found. Fig. (6) gives a quick means of finding the length of stabilizer span in the

slipstream. The parameter U is this length divided by the propeller diameter. The length in feet is DU and the fraction of the stabilizer span in the slipstream is $DU/2z_t$. Assuming a trapezoidal planform for the stabilizer, Fig. (7) shows a plot of G which is the fraction for the stabilizer area corresponding to the fraction of the span $DU/2z_t$ measured from the tip inward. This procedure for finding G takes into account the rotation mode of the propellers and the fact that in general both stabilizer ends will be immersed in the slipstream.

Stabilizer Lift and Pitching Moment. A horizontal stabilizer in a propeller slipstream is subjected to a flow pattern complicated by the presence upstream of a lifting wing. This pattern changes as the angle of attack of the airplane varies and the stabilizer and slipstream move through vertical displacements.

In previous sections the nature of the flow near a stabilizer was discussed and a means of calculating it presented. The relative location of the center of the slipstream and the tip of the stabilizer is given by v and h. With the aid of Figs. (6 and 7), G can be found.

The normal force coefficient of the stabilizer will first be calculated neglecting rotation and then the effect of rotation added. For the first part of the calculation a first order strip theory will be used. The lift distribution of the stabilizer in undisturbed flow will be approximated by a trapezoid with the taper ratio of the stabilizer. In the region of increased velocity the local section normal lift force is increased by a factor $(V/V_o)^2$. Ref. (20) carries out calculations for a wing with linearly varying velocity by a complete lifting line theory and the results are in excellent agreement with the assumption just mentioned. The following sketch illustrates the assumptions.

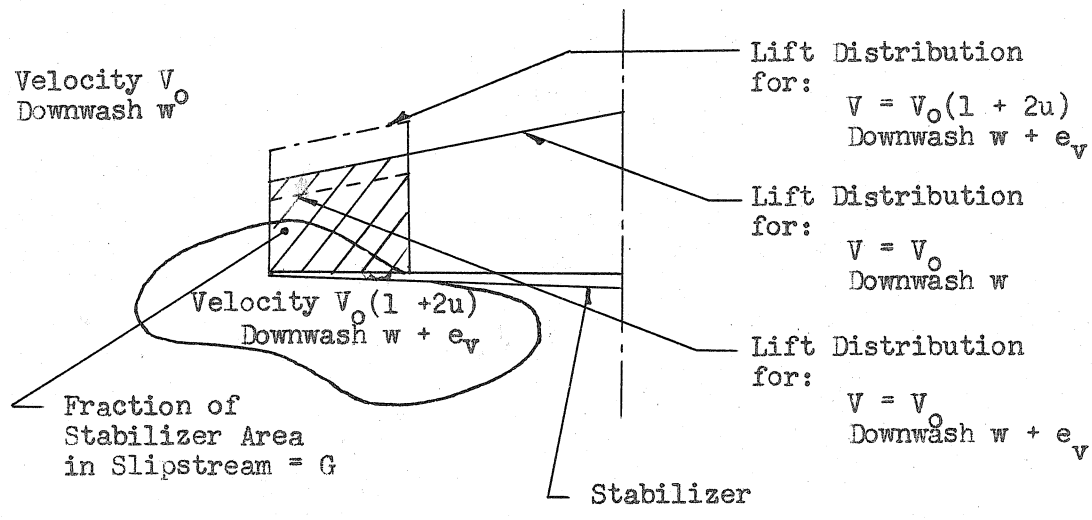

The lift coefficient of the portion of the stabilizer outside the slipstream is:

$$a_t \eta_t (\alpha + i_t + Ke - w)(1 - G)$$

For the fraction of the stabilizer in the slipstream, neglecting rotation, the lift coefficient is:

$$a_t \eta_t (1 + 8T_c/\pi)(\alpha + i_t + Ke - w - \lambda e_v)(G)$$

In this equation λ is a factor included to permit an experimental investigation of the assumptions concerning the inclination of the slipstream. It is evaluated for the five airplanes whose characteristics are computed in Sec. IV and a value of 1.2 is recommended. This evaluation will be discussed in Sec. IV.

For computing stabilizer normal force coefficients, a_t is the slope of the stabilizer lift vs. angle of attack curve for the isolated stabilizer. Ref. (21) gives values for a_t as obtained by lifting surface theory for low aspect ratio surfaces with elliptical planforms. In Ref. (22) these results are compared with experiments on a large number of isolated stabilizers of various planforms. The curves of

Fig. (8) are obtained from Ref. (21) and it is estimated in Ref. (22) that their accuracy is within 10% for conventional types of stabilizers.

η_t is the stabilizer effeciency factor for the power off condition. It is obtained by experiment, experience or simply estimated.

Adding the above two expressions together gives the stabilizer normal force coefficient without rotation:

$$C_{N_{t(\text{no rotation})}} = a_t \eta_t \left[(\alpha + i_t \text{ Ke} - w)(1 + G8T_c/\pi) - \lambda e_v G(1 + 8T_c/\pi) \right]$$

In computing the effect of rotational velocities somewhat different assumptions concerning the axial velocity field are indicated. Comparison of Fig. (4a) and Fig.(4b) shows that the rotational velocities are not confined to the inside of the slipstream. Around the outside of the slipstream there are rotational velocities which are in the opposite direction to those inside. This effect can be predicted qualitatively by the vortex propeller theory. Since the region of rotation and the region of increased axial velocity do not coincide, the prediction of their effect is greatly complicated. Also the parameter which describes rotation is valid only within the slipstream. A purely arbitrary assumption will be made concerning the effect of rotation and the validity of the assumption must be checked experimentally.

For the effect of rotation it will be assumed that the increased velocity field extends anywhere that rotation is present. The effect of the rotation on the stabilizer normal force coefficient will be the integral of the vertical flow angle caused by rotation over the span of the stabilizer divided by the stabilizer span. This integral will represent the mean angle of downwash caused by rotation and will be a function of v, h, and $C_p/J^2(1 + 8T_c/\pi)$ and different for each rotation mode. The following sketch illustrates the meaning of the integral:

Actual rotation configuration. All lengths dimensionless in terms of D.

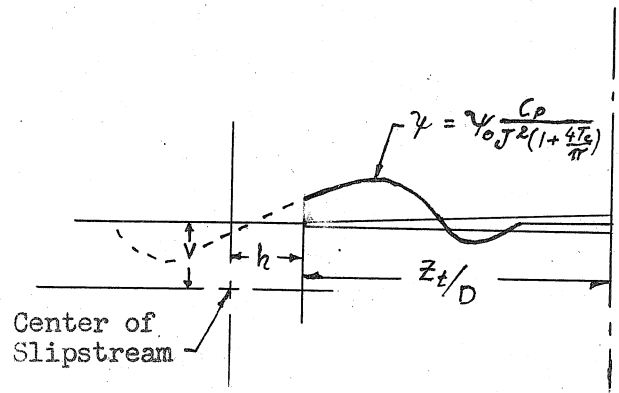

Equivalent rotation system. Actual lengths shown.

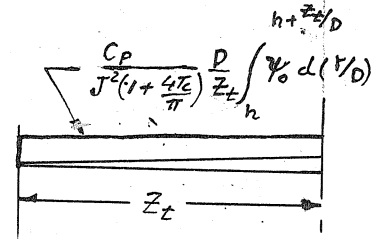

The integral defines a quantity H(v,h):

$H = \int \psi_0 (r/D)\, d(r/D)$ Integration is carried out over the entire stabilizer span.

H is plotted as a function of v and h in Fig. (5) for two rotation modes and instructions for single engine computations given. It should be noted that both slipstreams which act on the stabilizer of a multi-engine airplane are taken into account in the form of H which is given in Fig. (5).

The stabilizer normal force coefficient resulting from rotation is then:

$$a_t \eta_t \, (1 + 8T_c/\pi)(C_p/J^2(1 + 4T_c/\pi)(D/2z_t)H = a_t \eta_t C_p DH(1 + 4T_c/\pi)/J^2 2z_t$$

The total stabilizer normal force coefficient is obtained by adding the separate parts:

⑮ $$C_{N_t} = a_t \eta_t \left[(\alpha + i_t + Ke - w)(1 + 8GT_c/\pi) - \lambda e_v G(1 + 8T_c/\pi) + C_p DH(1 + 4T_c/\pi)/J^2 2z_t\right]$$

where e_v from Equation ⑩

$w = m + kC_L$

H — from Fig. (5) using v from Equation (13) and h from Equation (14).

G — the fraction of the stabilizer area in the slipstream is obtained as follows:

1. Obtain U from Fig. (6) using v and h.
2. Obtain G from Fig. (7) using $DU/2z_t$ and the taper ratio of the stabilizer.

k — elevator effectiveness $\Delta i_t/e$

e — elevator deflection.

From this the stabilizer pitching moment coefficient is :

(16) $C_{M_t} = -C_{N_t} x_t S_t/Sc$

IV CALCULATION OF POWER-ON STABILITY

The following procedure is planned for tabular calculation. For most applications curves of C_L vs. α and C_M vs. C_L will be desired for a series of flight power conditions at various elevator deflections. Since the C_M vs. C_L curve is not straight with power-on, the trim condition ($C_M = 0$) gives the only value of ($- dC_M/dC_L$) which has a physical significance for steady state flight.

In order to calculate the power-on C_L vs. α and C_M vs. C_L curves, all necessary physical dimensions of the airplane must be known, the power-off curves must be known or estimated for both the tail-on and tail-off configurations and the power conditions and propeller characteristics given.

Angle of attack is the most convenient independent variable because C_L is a function of power and must be calculated from C_{L_o} for chosen values of α.

C_L vs. α Curve.

In computing the total lift coefficient for a chosen angle of attack, the direct propeller forces and the lift increment due to the slipstream passing over the wing are added to the lift coefficient of the complete airplane power-off. This procedure makes the calculation of C_L as a function of α a very rapidly converging sucessive-approximation process. Consideration of the changes in lift of the stabilizer due to power in finding C_L would make the computation of C_M as function of C_L a double sucessive approximation and it is not recommended. In this report the lift of the stabilizer will be assumed to be equal to the unpowered value for a specified α in computing C_L.

C_L for a chosen value of α may be calculated as follows:

$$(17) \qquad C_L = C_{L_o} + \Delta C_L + \sum_{i=1}^{E} T'_{c_i} (\alpha + i_{p_i}) + \sum_{i=1}^{E} R_i (\alpha + i_{p_i})$$

where: subscript i designates number of propeller for 4 or 6 engine aircraft.

Procedure:

1. Find C_{L_o} for the chosen value of α from power-off, tail-on curves.
2. Estimate the value of C_L.
3. Find T'_c, T_c, C_T and J for the estimated C_L.
4. Find R from Equation 4 and Fig. (2) using J, C_T, and the propeller blade planform.
5. Calculate e_v from Equation (10) using Fig. (3) and R, T_c, and .
6. Calculate ΔC_L from Equation (12).
7. Calculate C_L from Equation (17) using C_{L_o}, ΔC_L, T'_c, R and α as obtained above.
8. If C_L as calculated agrees with the estimated C_L from step 2., then it is a correct value. If it does not agree use the calculated value as a second approximation and repeat until closure. This process will usually converge on the second try.
9. Repeat procedure for other values of α.

C_M vs. C_L Curve.

Once the C_L vs. α curve has been established for a specified power condition, the determination of C_M as a function of C_L is a direct calculation. It is a considerable simplification here to choose values of α and the calculated values of C_L which were determined in previous calculations in order to use values of variables which have been calculated.

$$(18) \qquad C_M = C_{M_o} + \sum_{i=1}^{E} \frac{R_i(\alpha + i_{R_i})A_{p_i}}{c} - \sum_{i=1}^{E} \frac{T_{c_i}' B_{p_i}}{c} - \frac{C_{N_t} S_t x_t}{Sc}$$

where: subscript i designates number of propeller for 4 or 6 engine aircraft

Procedure:

1. C_L, T_c', T_c, R, and e_v are known for the values of α used in claculating C_L.
2. C_{M_o} is the tail-off, power-off pitching moment coefficient corresponding to values of α. The power-off, tail-off C_M curve is usually plotted against C_L. This C_L is not C_{L_o} because the tail contributes to the lift coefficient. The value of C_{M_o} must be found by determining the tail-off power-off C_L for a chosen value of α and then finding C_M for that C_L.
3. Use the same expression for w as was used to find the power-off tail pitching moment. Use the power-on C_L to find w.
4. Calculate v and h from Equations (13) and (14).
5. Find H from Fig. (5) using v and h.
6. Find U from Fig. (6) using v and h.
7. Find G from Fig. (7) using $DU/2z_t$ and the taper ratio of the stabilizer.
8. Use the same a_t (from Fig. (8), Ref. (22, 23, 24) or elsewhere), k, and η_t as were used in the power-off analysis.
9. Calculate C_{N_t} from Equation (15).
10. Calculate C_M from Equation (18).
11. Repeat for other values of α with the same power conditions and elevator deflection. This will give a curve which may be faired and $(-dC_M/dC_L)$ obtained graphically.
12. Repeat process for other elevator deflections if desired. The value of C_{N_t} is the only variable affected by elevator deflection.
13. Repeat process for other power settings. A new C_L vs. α curve

must be calculated for each new power setting.

Discussion of Results.

Calculations based on Equations (17) and (18) were carried out in order to obtain C_L vs. α and C_M vs. C_L curves which are compared with experimental curves of five airplane models for which adequate wind-tunnel data are available.

Description of Test Data: The wind-tunnel tests were conducted in the closed working section of the GALCIT[1] ten foot wind tunnel. Airplane No. 5 was tested with wire rigging and the other four models with a three-strut support system. The usual wind tunnel wall corrections for a circular closed section were made as a part of the GALCIT reports from which the data were taken. Experimental test points which are compared with calculated curves in this report are copied directly from the GALCIT reports. The dynamic pressures at which the tests were run are 10 or 15 gm/cm^2. All power runs are matched power with all engines operating and delivering the same power.

Wind-tunnel models were supplied by the Consolidated Vultee Aircraft Co. Airplane No. 2 was tested for the Vultee Field Division and the other four airplanes for the San Diego Division. Dimensions, propeller characteristics, center of gravity location, angular settings and power settings for these models were specified by Consolidated Vultee, incorporated into the GALCIT reports on the tests and copied from the GALCIT reports for this report. Propeller characteristic data given in the GALCIT reports were insufficient for the rotation analysis for airplanes No. 1, 2, and 3. The missing data were obtained from Ref. (25). The references cited contain the tested characteristics of propellers with approximately the same activity factors, blade section and blade twist distribution as the model propellers for the

[1] Guggenheim Aeronautical Laboratory, California Institute of Technology

airplanes mentioned. Errors in agreement between test and calculated curves which might be caused by differences in propellers will be discussed in the general analysis of the results. Three view sketches of airplanes No. 1, 2, and 3 are shown in Figs. (9, 10, 11). Dimensions needed for calculations are tabulated in Fig. (17) for these three airplanes. Airplanes No. 4 and 5 are not shown in order to avoid the necessity of release of the data from the military service for which they were designed. Airplane No. 4 is a two-engine twin-tail monoplane flying boat. Airplane No. 5 is a four-engine land plane.

Discussion of C_L vs. α Curves from Equation (17): Calculated curves and test points of C_L as a function of α for power-on are shown in Figs. (12 to 16) for five airplanes. The dashed lines show the C_{L_o} vs. α curves which were used in calculating C_L.

In general the agreement of Equation (17) with test values is excellent. The effect of the assumption of using the power-off tail load for calculating the power-on C_L appears to be negligible. Figs. (12, 14, 16) indicate that propeller rotation mode does not have an appreciable effect on ΔC_L as was assumed.

Discussion of C_M vs. C_L Curve from Equation (18): Calculated curves and test points of C_M vs. C_L for power-on are shown in Figs. (12 to 16). The dashed lines show the power-off, tail-on curves used for calculations. Power-off, tail-off C_M vs. C_L and C_L vs. α test points (not shown) were used to obtain $C_{M_o}(\alpha)$. The power-off tail pitching moment coefficient was obtained as follows:

$$C_{M_{t(\text{power-off})}} = C_{M_{(\text{power-off, tail on})}} - C_{M_o}$$

where: All values are for the same value of .

After $C_{M_{t(\text{power-off})}}$ vs. α was obtained, downwash at the stabilizer in the form $w(\alpha)$ was calculated assuming values of ηt and a_t.

Airplane No. 2 had a sufficiant number of different stabilizer settings to obtain w accurately by picking points where $C_{M_{t(power-off)}} = 0$. Using the C_{L_o} vs. α curve, the downwash angle was put into the form:

$$w = m + kC_L$$

Determination of the downwash angle permitted calculation of C_M from Equation 18 as outlined on page (34).

For the configurations with all propellers having right-hand rotation the general trends of all the computed curves follow closely the test points. Airplane No. 5 shows the worst agreement in Fig. (16). This may be partly because the value of i_p used in the calculations was of somewhat doubtful accuracy. Contradictory values of i_p appeared in two different places in the GALCIT report which gave the data for the airplane. The value finally used appeared to be the more logical and it was measured from a sketch. The other value would have yielded an even larger error than the one used. High thrust lines, low stabilizer location and small stabilizer incidence all tend to reduce the destabilizing effect of power at high angles of attack. However this airplane exhibits such a small effect of power on stability in the test results that none of these explanations is sufficient to explain it. The tail-off power-on characteristics agree very well with calculated results so the explanation is to be found in the tail pitching moment. Curves of C_M vs. C_L power-on for elevator deflected (not shown) indicate that the stabilizer is still in the slipstream at high angles of attack so that the vertical location of the slipstream in the calculations is correct. The only remaining explanation is some unexpected effect of the nacelles or wing-fuselage intersection on the flow near the stabilizer.

Airplanes No. 1, 2, 3 and 4 exhibit the usual effects of power-on stability. Calculations by means of Equation (18) predict this effect for all-right-hand propeller rotation with good accuracy. One important result of the calculations is that the contribution of the rotational

velocities in the slipstream for this rotation mode is neglegible as shown by the values of H obtained from Fig. (5). This seems reasonable since rotation produces an upward force on the right half of the stabilizer and a downward force on the left. For this rotation mode, the numerical value of H is a small difference of two slightly different quantities and is negligible.

The factor λ for all-right-hand-rotation is obtained by equating experimental values of C_{M_t} to Equation (16) which gives an expression with only λ as an unknown after all the known variables of the problem are substituted. This procedure was carried out for all values of for which calculations were made on airplanes No. 1, 2, 3 and 4. At high angles of attack λ came out 1.25, 1.20, 1.25, and 1.10 respectively for these four airplanes. Variation at lower angles of attack was not large and was mostly due to the fact that small differences of quantities which were not calculated to enough significant figures were used in solving for λ at low values of C_L. Computed curves in Figs. (12 to 16) are based on $\lambda = 1.20$ and this value appears to be representative of this rotation mode for conventional aircraft. It should be noted here that the computed curves of Figs. (12 to 16) are based on a value of λ which was obtained from the experimental data to which the computed curves are compared. Also the value is based on tests of only four airplanes. Further investigation is necessary in order to determine whether a value of 1.20 for λ is always applicable to this propeller rotation mode and even to establish whether it can be regarded as a constant for any operating condition. The data for airplane No. 5 shows that this value of λ is not always applicable although the reason for the disagreement in this case is not immediately obvious.

For opposite rotation of the inboard propellers there is no consistant agreement between the calculated curves and experiment. Airplane No. 1 has the most complete variation of rotation modes. Curves for up-in-the-middle and down-in-the-middle rotation show trends

which are opposite to the experimental values. The up-in-the-middle rotation for Airplane No. 3 exhibits the same erroneous calculated trend. Airplane No. 5 shows the proper trend for the up-in-the-middle rotation mode but the stability is wrong in the same manner as with all-right rotation.

This confused situation indicates that the analysis of this report is not reliable in predicting the effects of rotation in the slipstream. The all-right-hand rotation analysis indicates that the vertical location of the slipstream and its general shape and velocity distribution are correctly determined. It is apparently the effects of phenomena associated directly with rotation which are not properly calculated. The errors are too large to be explained by any error which could result from the choice of propeller characteristics where they were not specifically given in the GALCIT reports. Evidently these discrepencies are due either to improper simplifying assumptions in evaluating the effects of rotational velocities or to improper determination of properties of the slipstream which depend directly on rotation or both.

In defining H, the difficulty of the different regions of rotational velocity and increased axial velocity in the slipstream became evident. The assumption that the two regions are the same may lead to serious errors in the evaluation of H. It is also possible that a strip theory based on some assumption of the lift distribution of the stabilizer in undisturbed flow would lead to a better determination of H as a function of v and h. Spanwise flow over the stabilizer due to horizontal components of rotational velocities may cause important changes in the stabilizer normal force.

There is some experimental indication that an inclined slipstream drifts sidewards as it progresses downstream. No theoretical means of predicting this drift is available and reliable quantitative data are lacking. This effect may be important for opposite-rotating inboard

propellers. It would probably have very little effect for all-right-hand rotation because both slipstreams would deflect in the same direction and thus cause only slight changes in the fraction of the stabilizer immersed in the slipstream. The field of induced rotational velocity outside the slipstream has not been computed theoretically and downwash surveys can give only qualitative indication of the parameters which govern its distribution and magnitude. Although it is evident that the rotational velocities inside the slipstream will have a strong effect on the rotation outside, the nature of the effect is not entirely clear. Another possibility for error is that some nacelles, wing-fuselage intersections, thrust line locations or wing lift distributions so strongly influence the downwash distribution due to rotation in the slipstream that the approach to predicting the effects of rotation in this report may be invalidated entirely by certain airplane configurations.

In general it appears that the means of predicting the effects of rotation in the slipstream on stability suggested in this report is not sufficiently accurate for design purposes.

V DESIRABLE CONFIGURATION FOR POWER-ON STABILITY

The undesirable effects of power-on static longitudinal stability usually appear most pronounced at high lift coefficients. This phenomenon has two basic reasons. First, the thrust coefficients which describe the propeller effects on stability increase with increased C_L. Second, the angle between the propeller axis and the relative wind increases with increased C_L. The direction of inboard propeller rotation also has a pronounced effect on stability because of flow at the stabilizer.

The following recommendations will usually improve static longitudinal stability at high lift coefficients:

1. The thrust axis should be inclined downward so that it is parallel to the relative wind at as high a lift coefficient as possible. This does not decrease the lift coefficient at lower angles of attack due to the downward component of the thrust as might be expected. Experiments in Ref. (7) show that the effect of the increased local angle of attack in the slipstream almost exactly balances the downward thrust component giving a constant C_L over a wide range of thrust axis inclination. This improvement is limited by the possibility of local stalling of the wing behind the propeller blades which are moving upward or early separation in the same region with laminar flow airfoils.
2. The most desirable propeller rotation mode is with the inboard propellers rotating in opposite directions and the inboard blades moving upward. This configuration causes the rotation in the slipstream to improve stability for aircraft where the stabilizer span is about the same as the distance between the inboard propeller hubs. There is often

a slight increase in C_L with this rotation mode because of a better spanwise lift distribution over the wing in the region of the fuselage. The case of both inboard propellers rotating in the same direction usually has very little effect on stability from rotational flow in the slipstream. Co-axial counter-rotating propellers presumably have no rotational components of flow in the slipstream although this case was not investigated and no experimental data are included among the references cited this report. Opposite-rotating inboard propellers with the inboard blades moving downward have a very destabilizing effect and it is recommended that they not be used for aircraft of the general configuration considered in this report. For tailless aircraft the direction of propeller rotation would presumably not have any affect on static longitudinal stability except perhaps the interference effect with the nacelles which is not subject to prediction by numerical calculation methods.

3. The stabilizer should be located as low as possible in an effort to place it below the slipstream at high lift coefficients. This is more easily accomplished if the thrust axis is inclined downward. The region below the slipstream has an appreciably smaller angle of downwash than that above it where the wing wake is most pronounced and the velocity is decreased by flow over the wing. Ref. (5) gives the results of tests on a twin-engine model with the stabilizer in three vertical positions and the low position yields the best stability. Wake surveys in Ref. (6, 7, 16) show the same results. It should be mentioned in the interest of objectivity that Ref. (26) gives the results of tests on a single-engine low-wing monoplane with the stabilizer in

three vertical positions and the highest position gives best stability. Possibly the flow near the fuselage would invalidate this result as it concerns multi-engine aircraft. There is some indication that a low stabilizer position is undesirable for the flaps deflected configuration due to the change in the zero lift line and the wing wake position. The wake surveys which show the flow behind flapped wings are so confusing that no general conclusions can be drawn. The limitation in lowering the stabilizer is the possibility of buffeting from the wing wake or exciting natural vibration modes by oscillating velocity components in the slipstream.

4. Stabilizer incidence with respect to some wing reference direction (root chord line, zero lift line, etc.) should be as positive as possible. This result was obtained theoretically in Ref. (27) but its magnitude could not be determined by the methods used. The reason for this effect is that there are two dominant effects of the slipstream on the stabilizer besides rotation. One is the inclination of the slipstream due to the inclined propeller. This effect always gives a more positive pitching moment than the power-off case and can be minimized by tilting the thrust axis or moving the stabilizer out of the slipstream. The other effect is the increased velocity which increases the effectiveness of the stabilizer. This is clearly a function of the stabilizer setting and a more positive stabilizer setting will improve stability.

VI RECOMMENDED TABULAR COMPUTATION PROCEDURE

In order to compute values of C_L and C_M for a series of angles of attack, some form of tabular procedure is necessary because of the large number of variables involved. It was found most convenient to carry out computations in three series in order to avoid duplications. Series 0 is used to collect the necessary data concerning the airplane itself in the form in which it will be needed. Series I is used to reduce operating parameters to a useful form and to find C_L. Series II is used to compute C_M.

The following recommended precedure applies only to the case of both inboard propellers with right hand rotation and symmetrical power. Other rotation modes have not been investigated sufficiently due mostly to lack of data. The results of computations which were made show bad agreement with tests. The case of unsymmetrical power has not been investigated because of lack of data.

Series 0: Airplane Characteristics.

Fig. (17) shows the numerical values of necessary dimensions and ratios for Airplanes No. 1, 2 and 3. The values have identification numbers [1] to [39]. All dimensions are in feet to model scale although full scale could be used since values appear in calculations only in dimensionless ratios. Note that x_p and y_p are for the inboard propellers only of four and six-engine airplanes. A_p and B_p must be shown for all propellers. Subscripts on A_p and B_p denote the number of propeller (left outboard propeller is No. 1 and counting is from left to right).

Series I: Calculation of C_L.

Fig. (18) shows calculations leading to a value of C_L for a chosen value of α for Airplane No. 1. The steps are [101] to [132].

Only enough decimal places are carried to give two places in the final answer because C_{L_o} and the power settings are only known to that accuracy. Values of C_{L_o} were found from the dashed line in Fig. (12) for selected values of α. The curve of T_c' vs. C_L from which T_c' was obtained appears in the GALCIT report for this airplane. Propeller characteristics were obtained from the T_c' vs. C_L curves, the propeller blade angle as given in the report and propeller charts from Ref. (25). Results are plotted as solid lines in Fig. (12).

This calculation is essentially a successive approximation procedure since C_L must be estimated in step [2] and then the value of C_L which is calculated compared to the estimate. This is such a rapidly converging process that a second try is almost never necessary to obtain two decimal place accuracy.

Series II: Calculation of C_M.

Fig. (19) shows calculations leading to a value of C_M for chosen values of α for Airplane No. 1. The calculation steps are [201] to [224]. Three decimal place accuracy in the final result was all that could be justified because of the data against which the calculations were checked. The downwash angle at the stabilizer was obtained as outlined on page (37). Note that the rotation factor, H, is not used because it was found to be negligible for the all-right-hand rotation case. Results are plotted as a solid line in Fig. (12).

With the calculations in this form it is easy to investigate how variations in any of the physical characteristics of the airplane can affect stability. The quantities which have the most noticeable influence are i_p, i_t, and y_t.

REFERENCES

1. Millikan, C.B.; J. Ae. S. Vol. 7, No. 3, January 1940
   The Influence of Running Propellers on Airplane Characteristics.

2. Durand, W.F.; January 1934
   Aerodynamic Theory, Vol. IV.

3. Hufton, P.A.; R.A.E. T.N. Aero. 1119, January 1943
   Propeller Forces Due to Yaw and Their Effect on Airplane Stability.

4. Rumph, L.B., White, R.J. and Grumman, H.R.; J.Ae. S.Vol. 9, No. 12, October 1942.
   Propeller Forces Due to Yaw and Their Effect on Airplane Stability.

5. Bryant, L.W. and McMillan, G.A.; A.R.C., No. 3603, June 1938
   The Longitudinal Stability of a Twin-Engined Monoplane with Airscrews Running.

6. Rogallo, F.M. and Swanson, R.S.; N.A.C.A. A.R.R., January 1943
   Wind-Tunnel Tests of a Twin-Engine Model to Determine the Effect of Direction of Propeller Rotation on the Static Stability Characteristics.

7. Stuper, J.; N.A.C.A. T.M., No. 874, August 1938
   Effect of Propeller Slipstream on Wing and Tail.

8. Sweberg, H.H.; N.A.C.A. A.R.R., August 1942.
   The Effect of Propeller Operation on Air Flow in the Region of the Tail Plane for a Twin-Engine Tractor Monoplane.

9. Smelt, R. and Davies, H.; R. and M., No. 1788, 1937
   Estimation of Increase in Lift Due to Slipstream.

10. Bradfield, F.B.; R. and M., No. 1488, June 1932
    Wind Tunnel Data on the Effect of Slipstream on the Downwash and Velocity at the Tailplane.

11. Goett, H.J. and Pass, H.R.; N.A.C.A. Report, May 1941
    Effects of Propeller Operation on Pitching Moments of Single-Engine Monoplanes.

12. Muttray, H.; N.A.C.A. T.M., No. 876, September 1938
    Investigations on Downwash Behind a Tapered Wing with Fuselage and Propeller.

13. Sweberg, H.H.; N.A.C.A. A.R.R., November 1942
    Full Scale Tunnel Investigation of the Control and Stability of a Twin-Engine Monoplane with Propellers Operating.

14. de Feriet, J.K. and Fauquet, A.; G.R.A. N.T., No. 2, March 1939
    Influence of Slipstream on Aerodynamic Characteristics of a Powered Model.

15. de Feriet, J.K. and Fauquet, A.; G.R.A. N.T., No. 4, May 1939
Influence of Slipstream on the Aerodynamic Characteristics of a Powered Model.

16. Katzoff, S.; N.A.C.A. Report, No. 690, 1940
Longitudinal Stability and Control with Special Reference to Slipstream Effects.

17. Ried, E.G.; N.A.C.A. T.N., No. 1040, July 1946
Wake Studies of Eight Model Propellers.

18. Burrington, R.S. and Torrence, C.C.; McGraw-Hill; 1939
Higher Mathematics.

19. Bell, R.W. and Storms, H.A., Jr.; GALCIT Thesis, 1941
Some Aspects of the Effects of Propeller Operation on the Static Longitudinal Stability of an Airplane.

20. Fejer, A.; Ph. D. Thesis, Cal Tech, 1945.
Lifting Line Theory in Linearly Varying Flow.

21. Swanson, R.S. and Crandall, S.M.; N.A.C.A. T.N. 1175, Feb. 1947
Lifting-Surface-Theory Aspect-Ratio Corrections to the Lift and Hinge Moment Parameters for Full-Span Elevators on Horizontal Tail Surfaces.

22. Bates, W.R.; N.A.C.A. T.N. No. 1291, May 1947
Collection and Analysis of Wind-Tunnel Data on the Characteristics of Isolated Tail Surfaces with and without End Plates.

23. Martinov, A. and Kolosov, E.; N.A.C.A. T.M., No. 941, May 1940
Some Data on the Static Longitudinal Stability and Control of Airplanes. (Design of Control Surfaces)

24. Silverstein, A. and Katzoff, S.; N.A.C.A. Report No. 688, 1940
Aerodynamic Characteristics of Tail Surfaces.

25. Biermann, D., and Gray, W.H.; N.A.C.A. A.R.R. No. 1291, May 1947
Wind-Tunnel Tests of Single- and Dual- Rotating Tractor Propellers of Large Blade Width.

26. Bolster, C.M.; J. Ae. S., Vol. 4, No. 10, August 1937
Effect of Slipstream on Longitudinal Stability of a Low Wing Monoplane.

27. Donlan, C.J.; N.A.C.A. A.R.R., November 1942
Some Theoretical Considerations of Longitudinal Stability in Power-On Flight with special reference to Wind-Tunnel Testing.

TABLE OF FIGURES

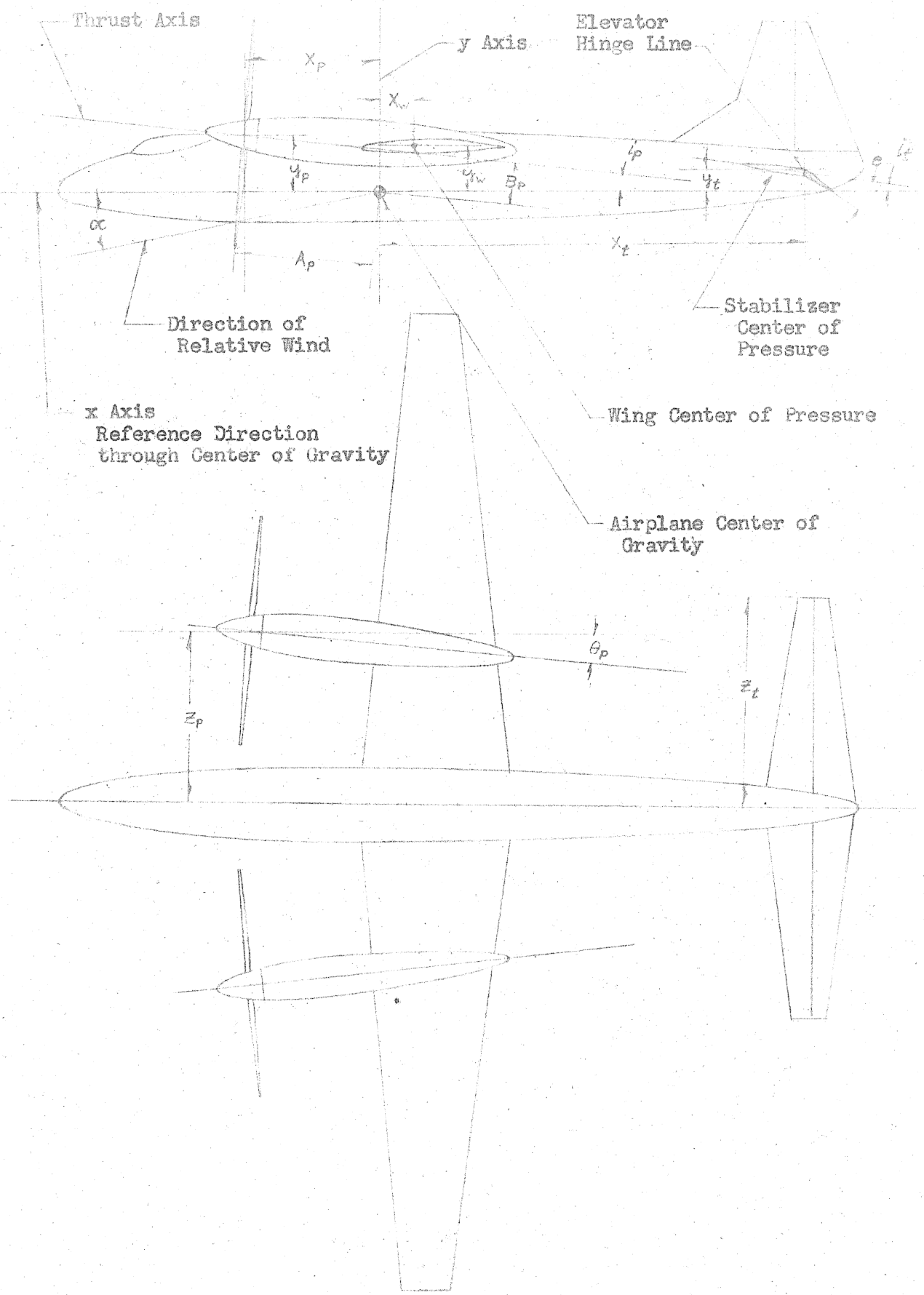

Fig. 1. Drawing Showing Dimensions and Angles.

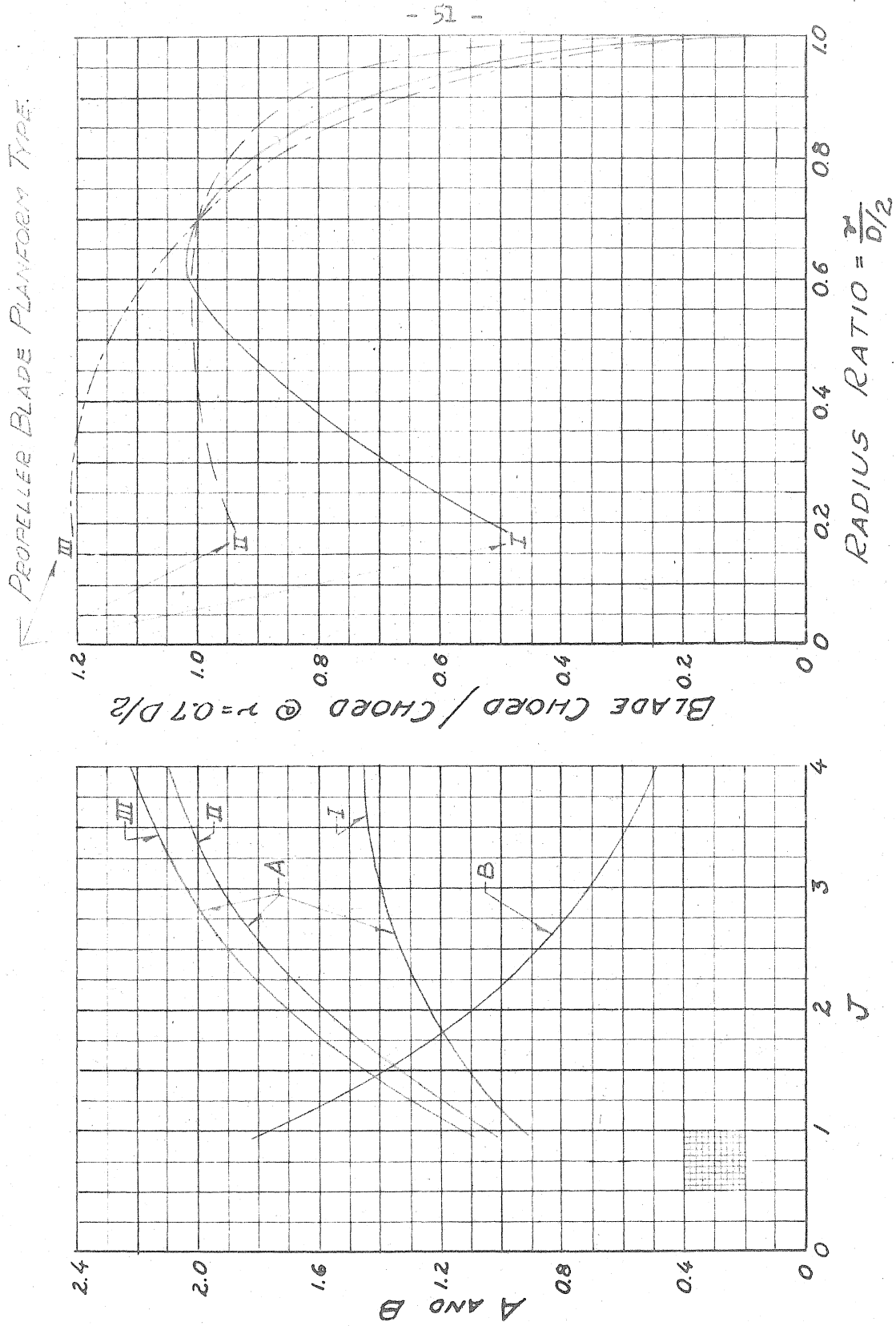

To find A and B for use in Equation 4 :

1. Select a propeller planform type which most nearly matches that of the propeller on the airplane.
2. Find A and B from curves for the appropriate planform type and for the J at which the propeller is operating.

Fig. 2. A and B as Functions of J and Propeller Planform.

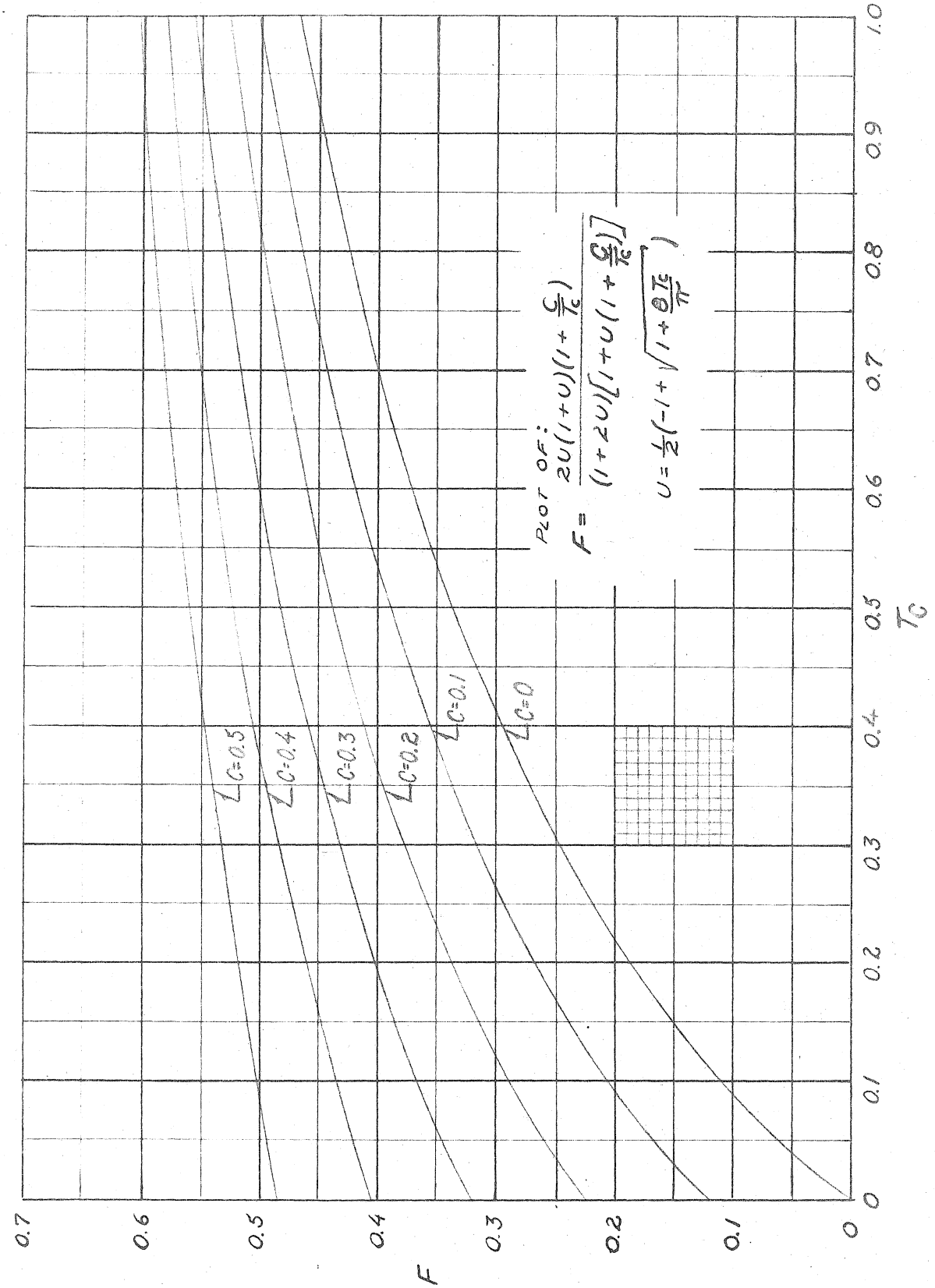

Fig. 3. F as a Function of T_c and C.

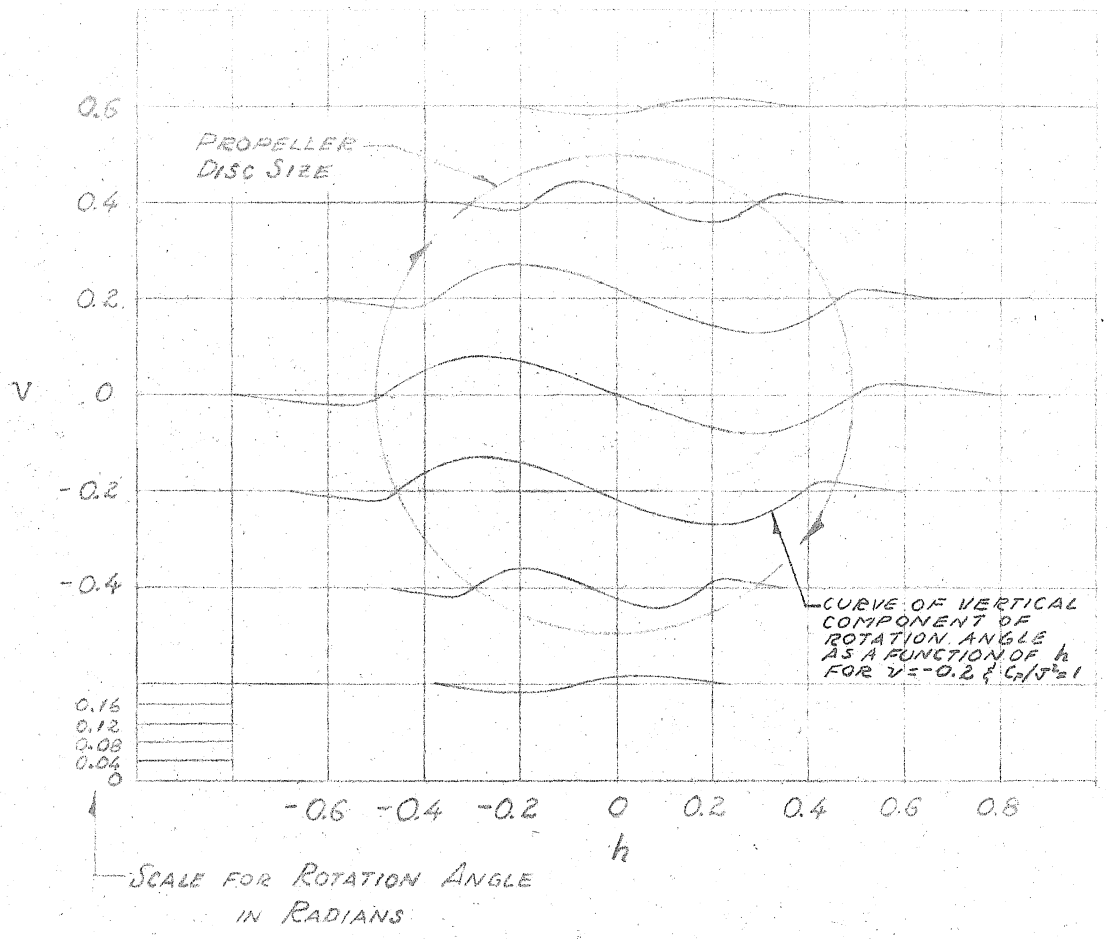

Fig. 4a. Distribution of Downwash Angle Due to Rotation in Slipstream.

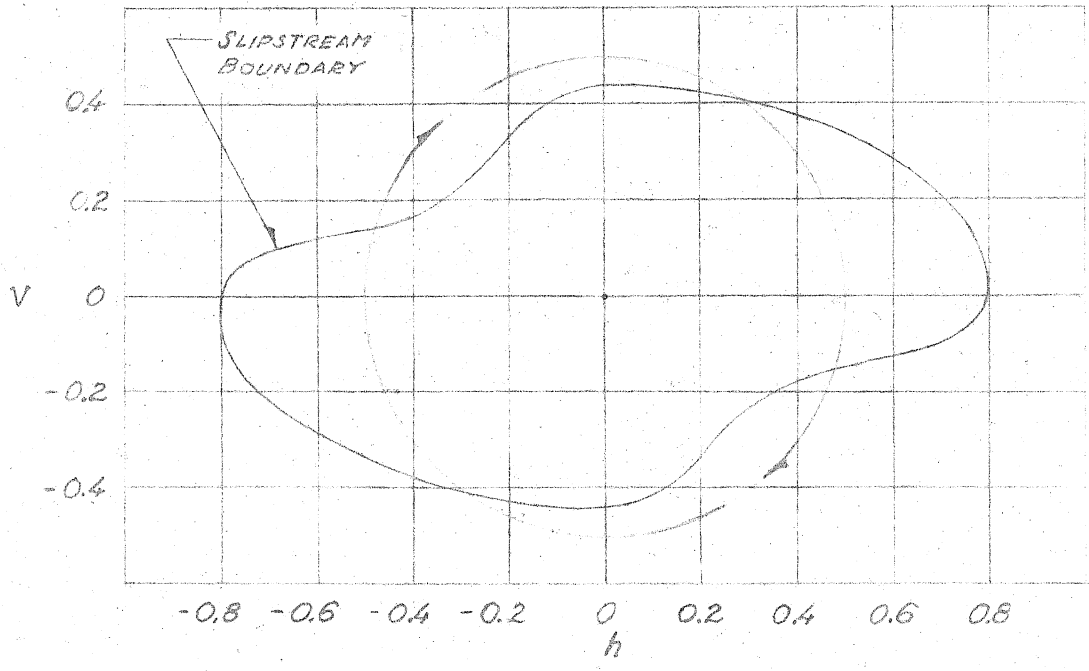

Fig. 4b. Shape of Slipstream at Stabilizer.

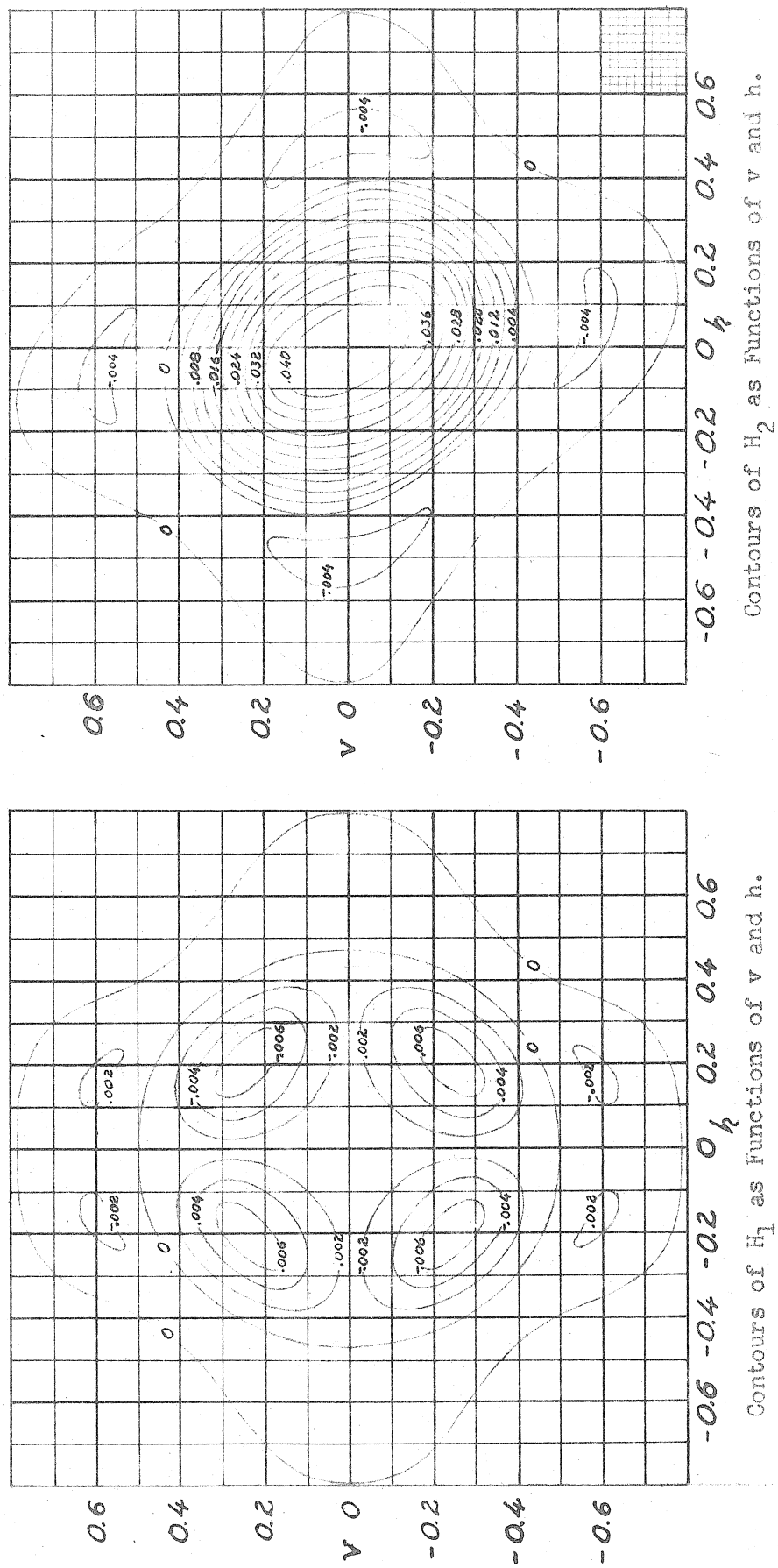

Procedure for finding H from v and h:

1. Find values of H_1 and H_2 from above curves.
2. For both inboard propellers with right hand rotation: $H = H_1$
3. For inboard propellers rotating in opposite directions and inboard blades moving up: $H = H_2$
4. For left inboard propeller feathered and right inboard propeller with right hand rotation: $H = H_2/2$
5. For right inboard propeller feathered and left inboard propeller with right hand rotation: $H = H_1 - H_2/2$
6. For right inboard propeller feathered and left inboard propeller with left hand rotation: $H = H_2/2$

Fig. 5. Curves and Procedure for Finding H as a Function of v and h.

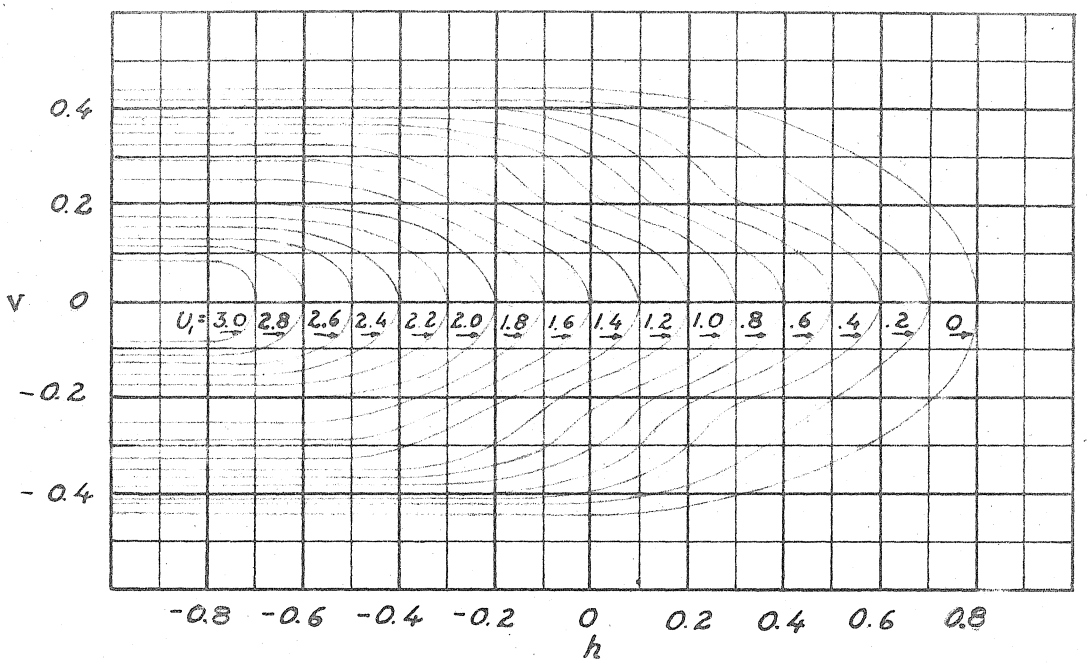

Contours of U_1 as Functions of v and h.

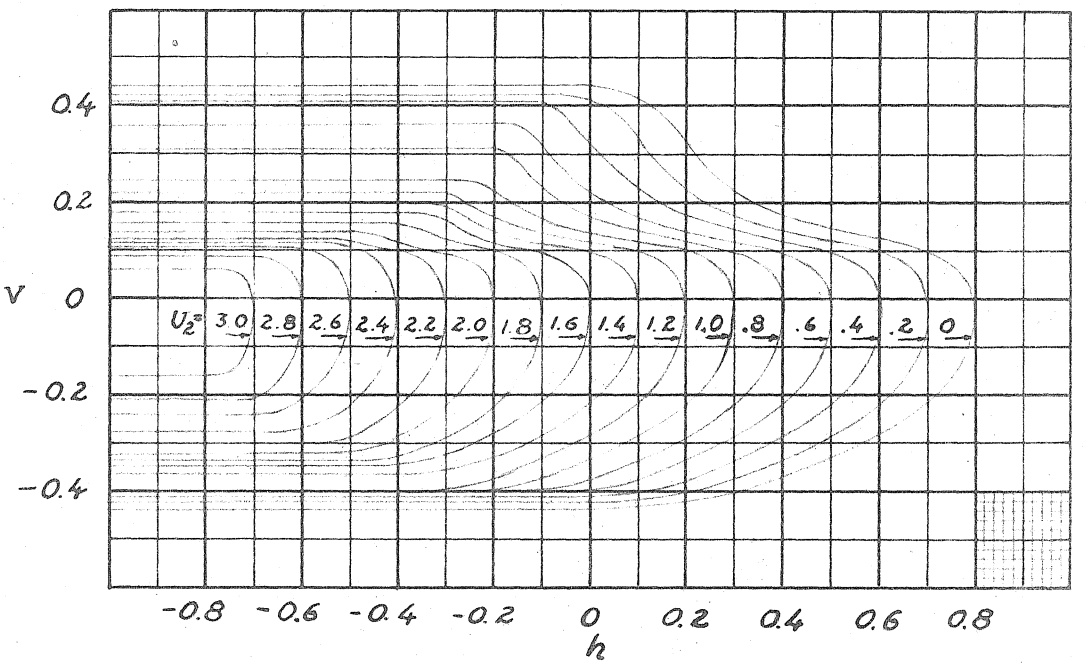

Contours of U_2 as Functions of v and h.

Procedure for finding U from v and h:

1. Find values of U_1 and U_2 from above curves.
2. For both inboard propellers with right hand rotation: $U = U_1$
3. For inboard propellers rotating in opposite directions and inboard blades moving up: $U = U_2$
4. For left inboard propeller feathered and right inboard propeller with right hand rotation: $U = U_2/2$
5. For right inboard propeller feathered and left inboard propeller with right hand rotation: $U = U_1 - U_2/2$
6. For right inboard propeller feathered and left inboard propeller with left hand rotation: $U = U_2/2$

Fig. 6. Curves and Procedure for Finding U as a Function of v and h.

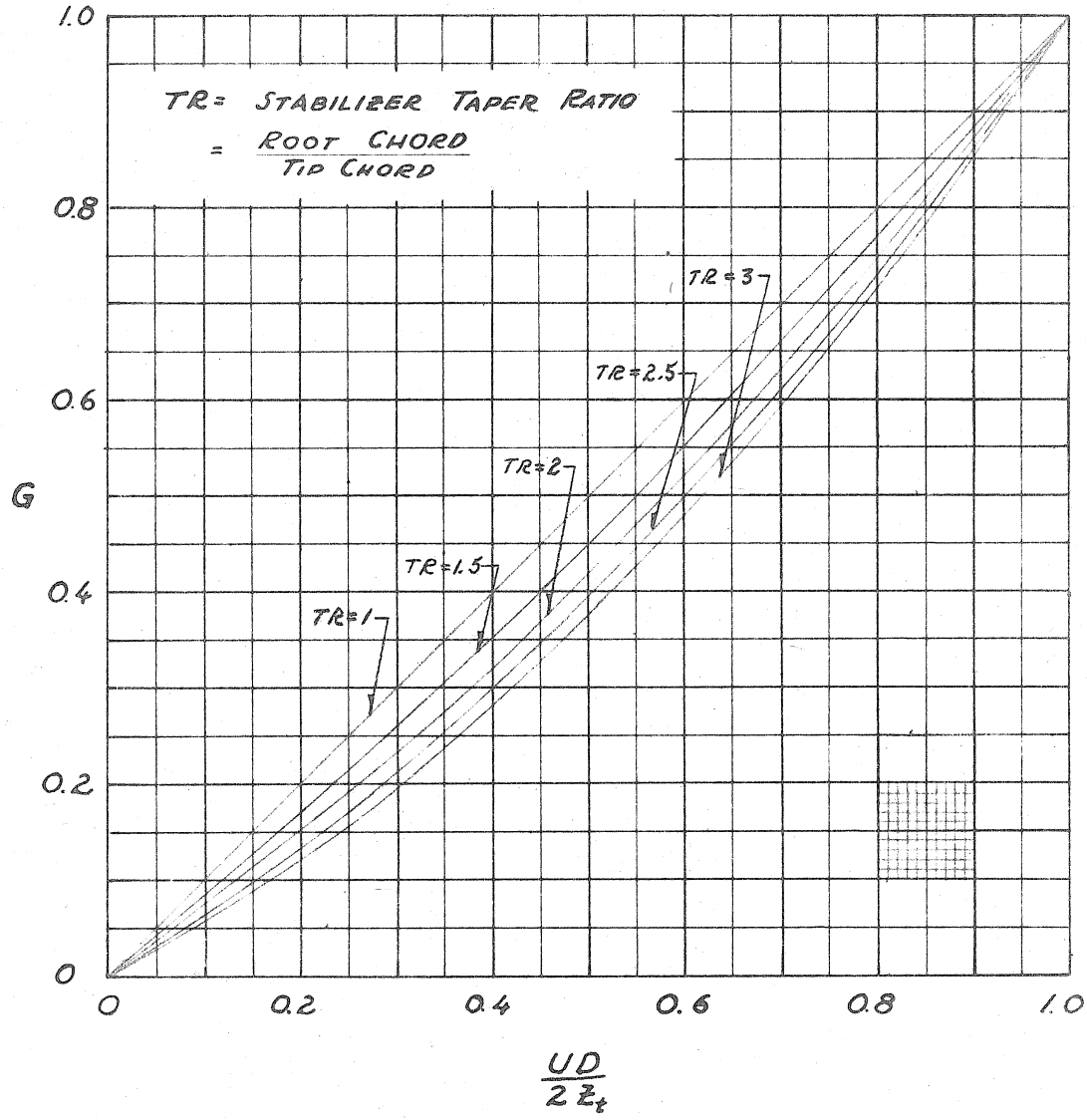

EQUATION:

$$G = \frac{\left(\frac{UD}{2Z_t}\right)\left[2 + \left(\frac{UD}{2Z_t}\right)(TR-1)\right]}{(TR+1)}$$

Fig. 7. Curves of G as a Function of U and Stabilizer Taper Ratio.

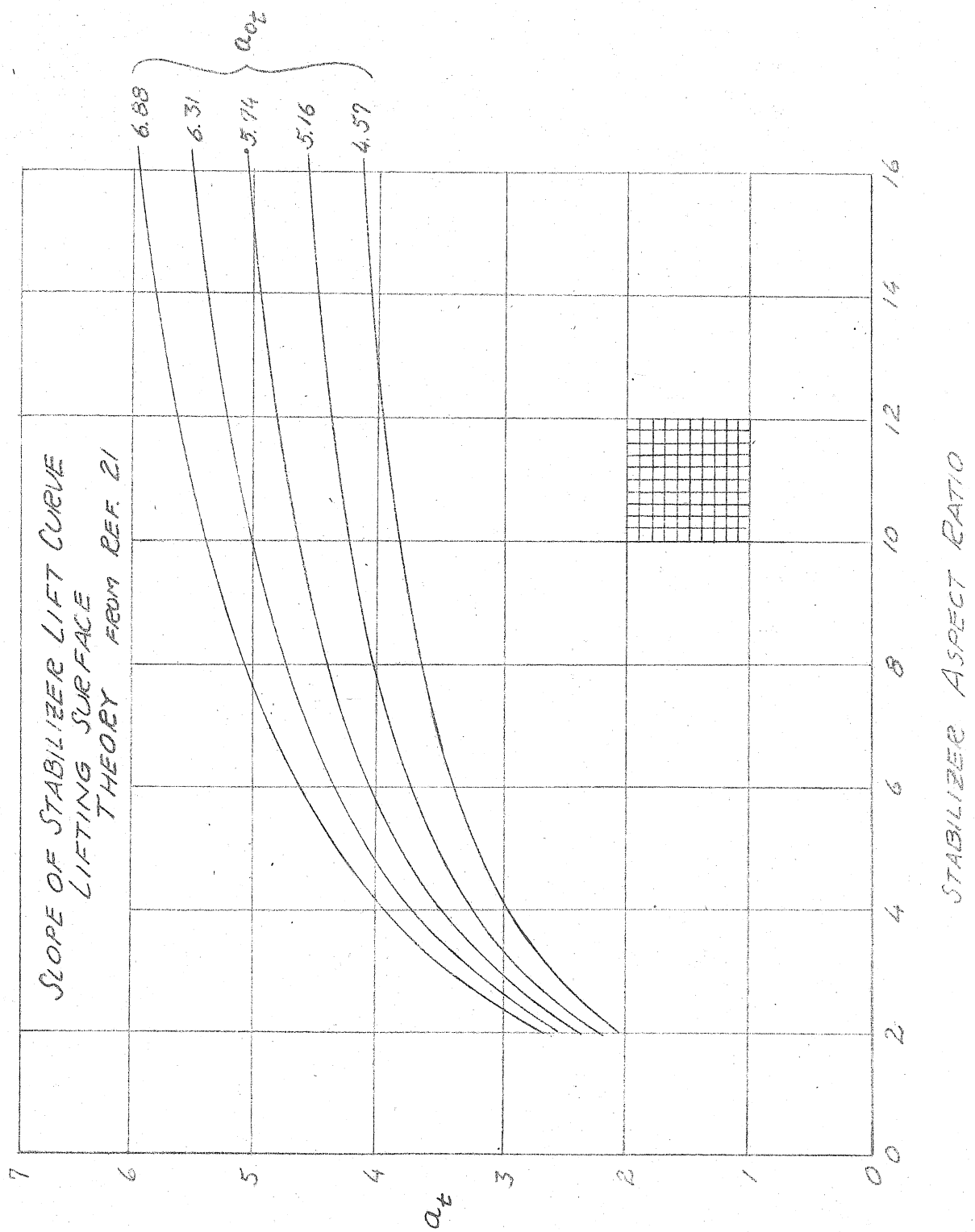

Fig. 8. a_t as a Function of a_{ot} and Stabilizer Aspect Ratio.

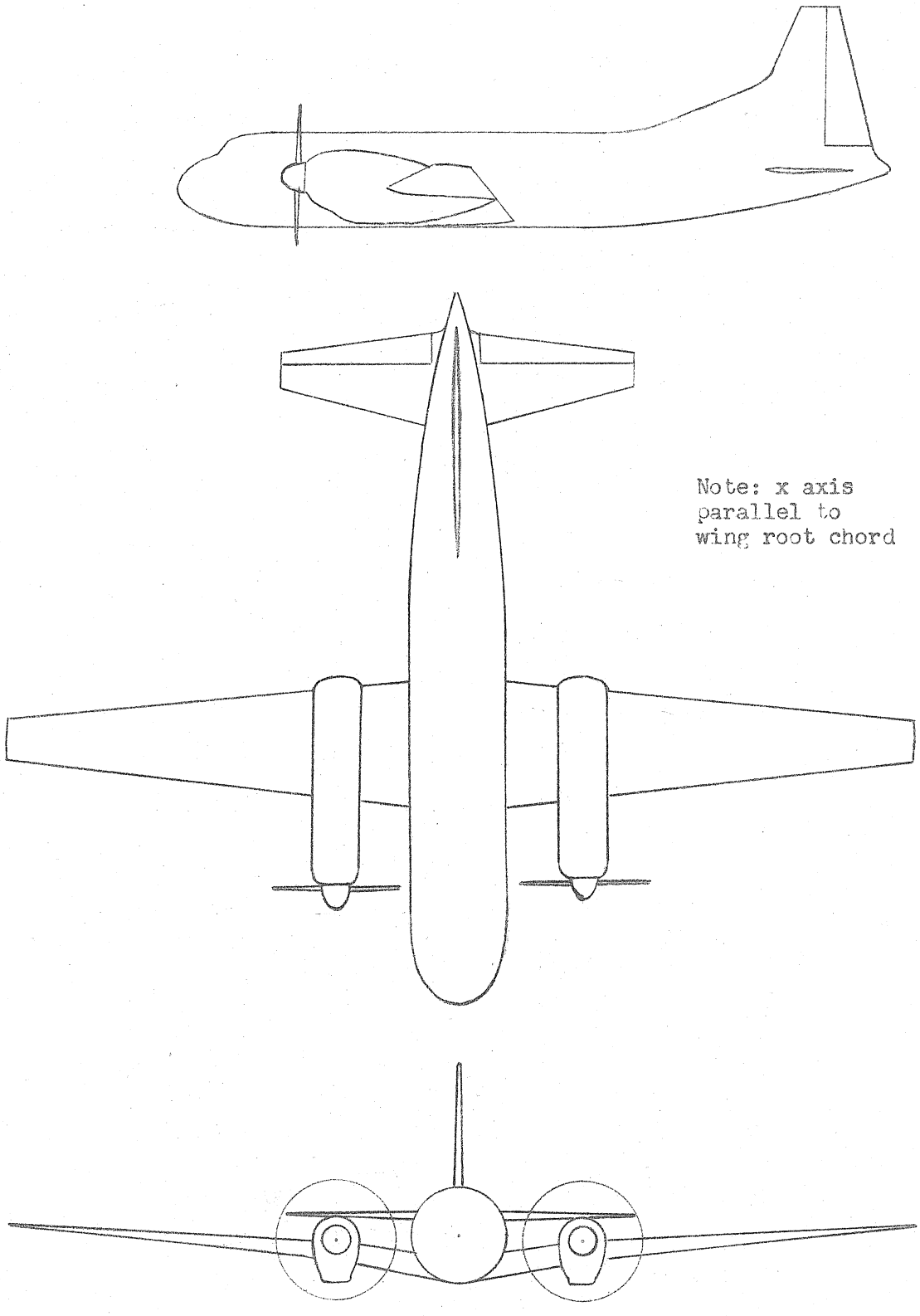

Fig. 9. Sketch of Airplane No. 1.

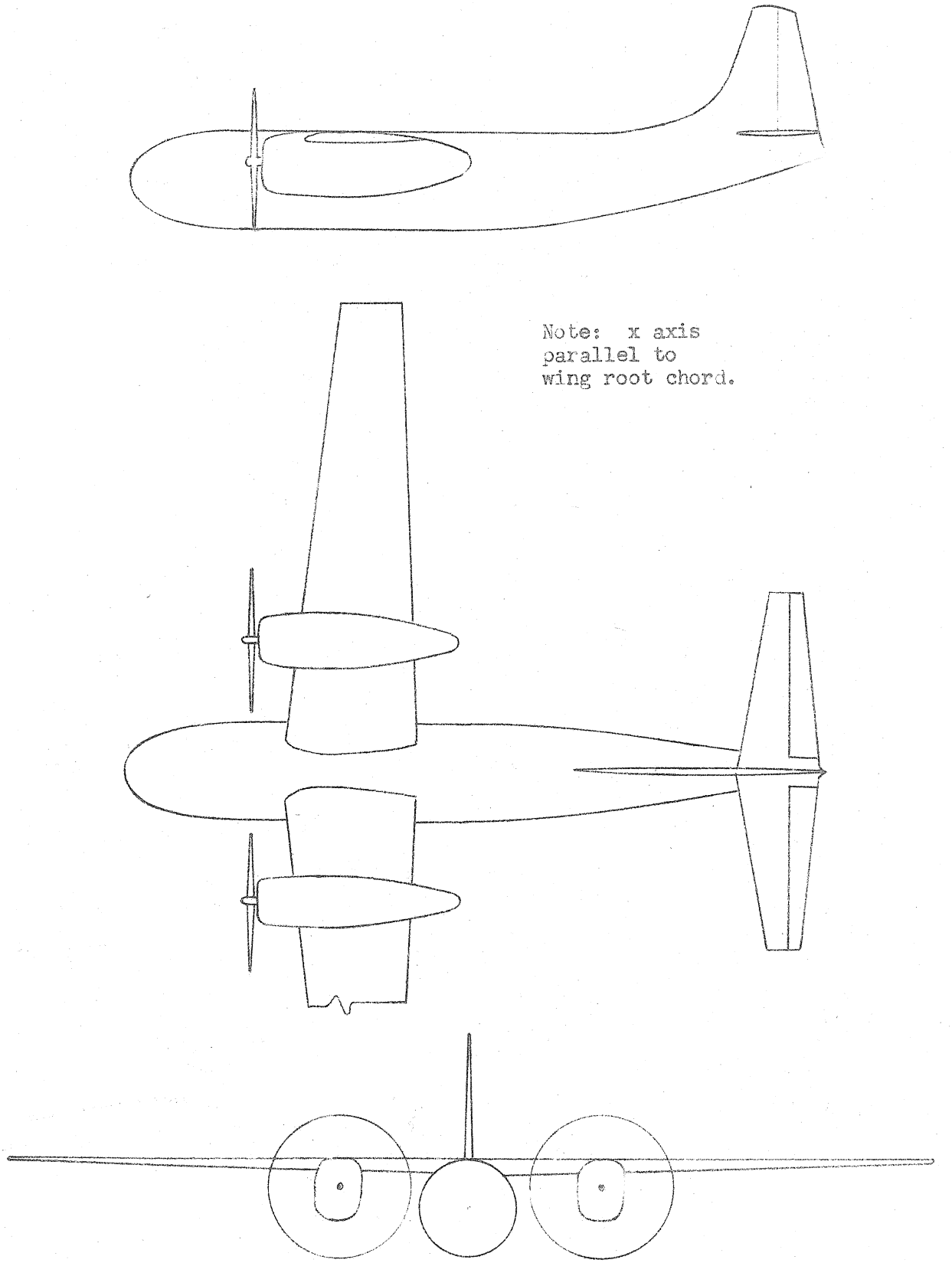

Fig. 10. Sketch of Airplane No. 2.

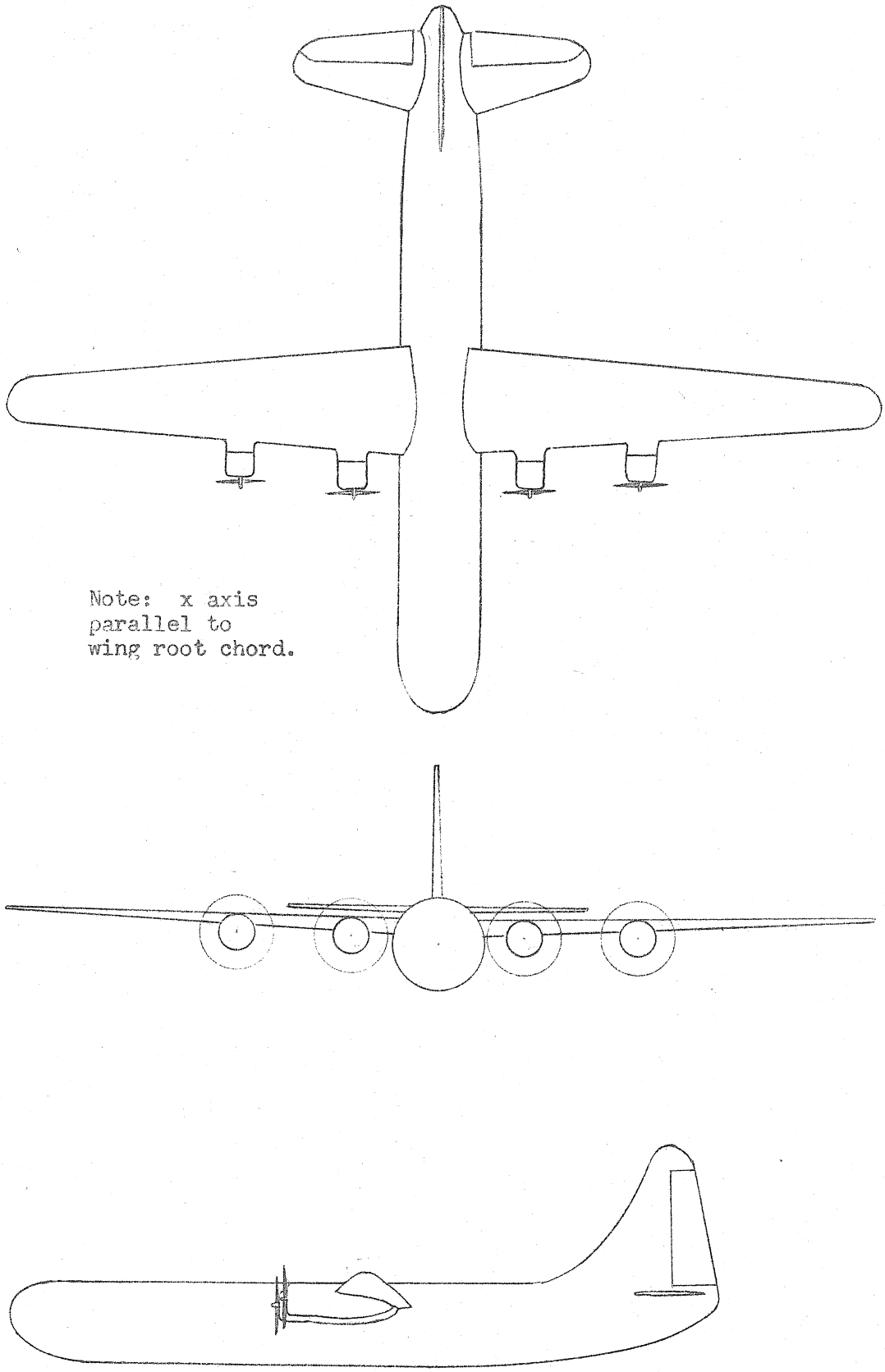

Fig. 11. Sketch of Airplane No. 3.

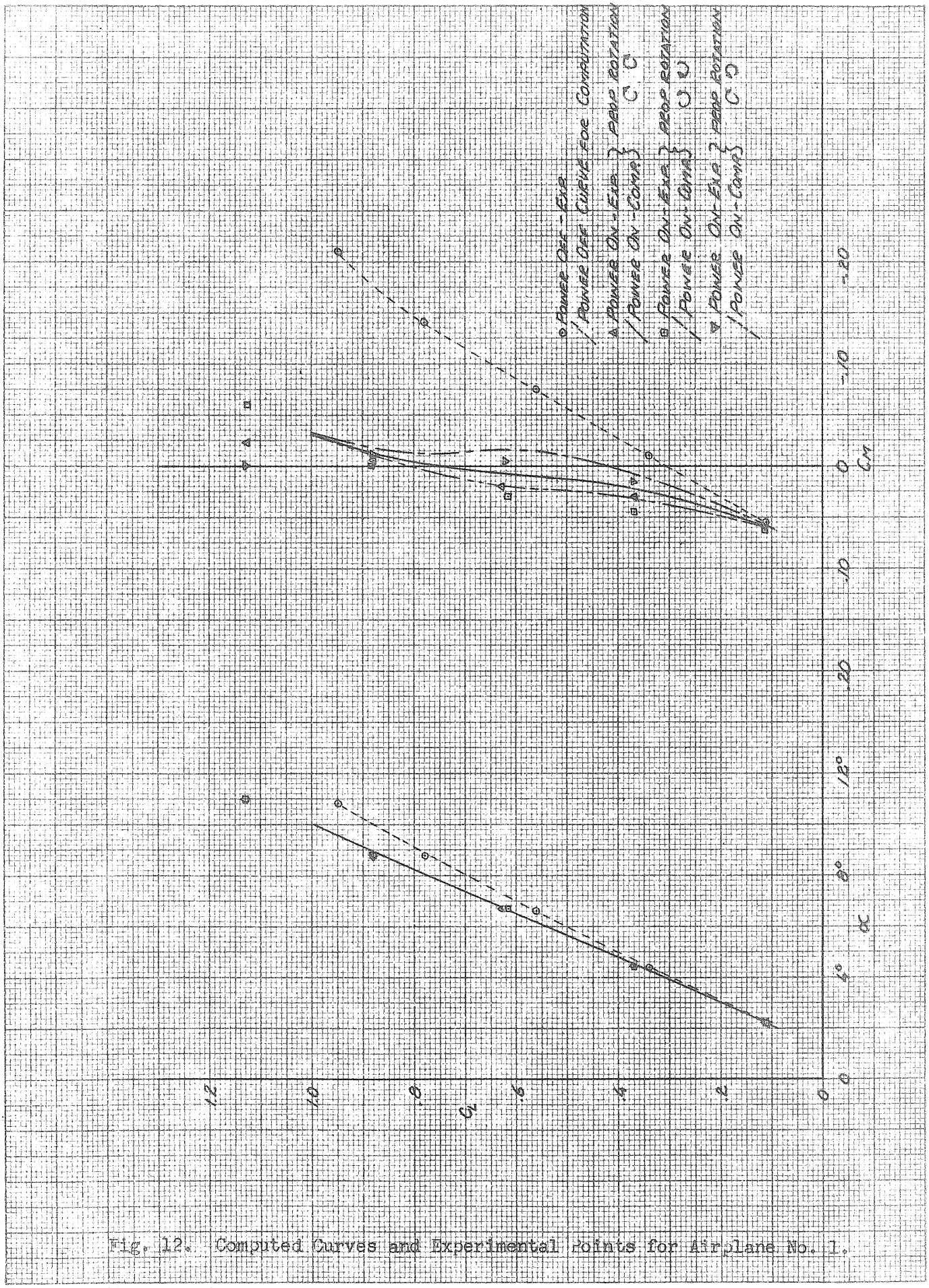

Fig. 12. Computed Curves and Experimental Points for Airplane No. 1.

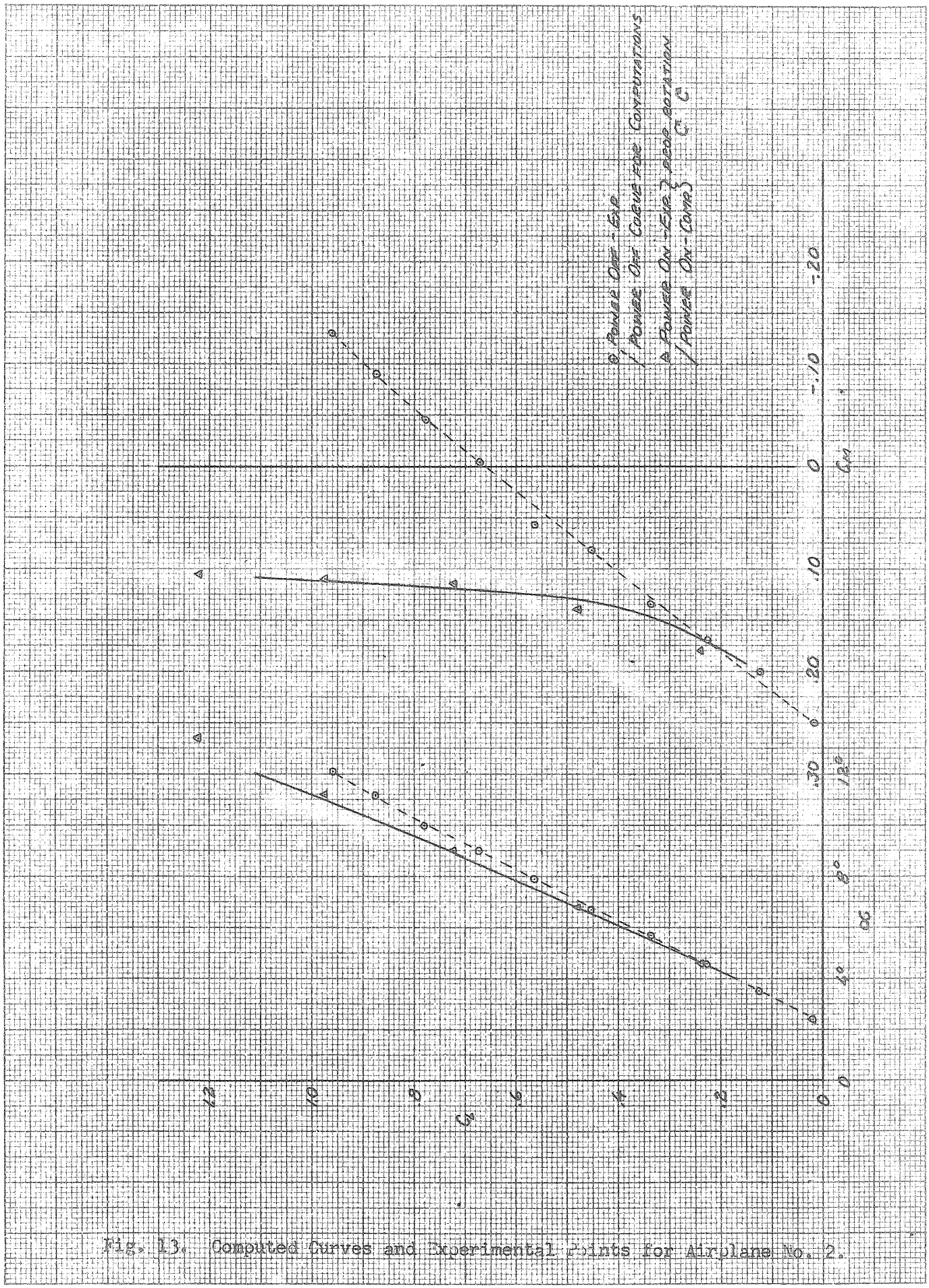

Fig. 13. Computed Curves and Experimental Points for Airplane No. 2.

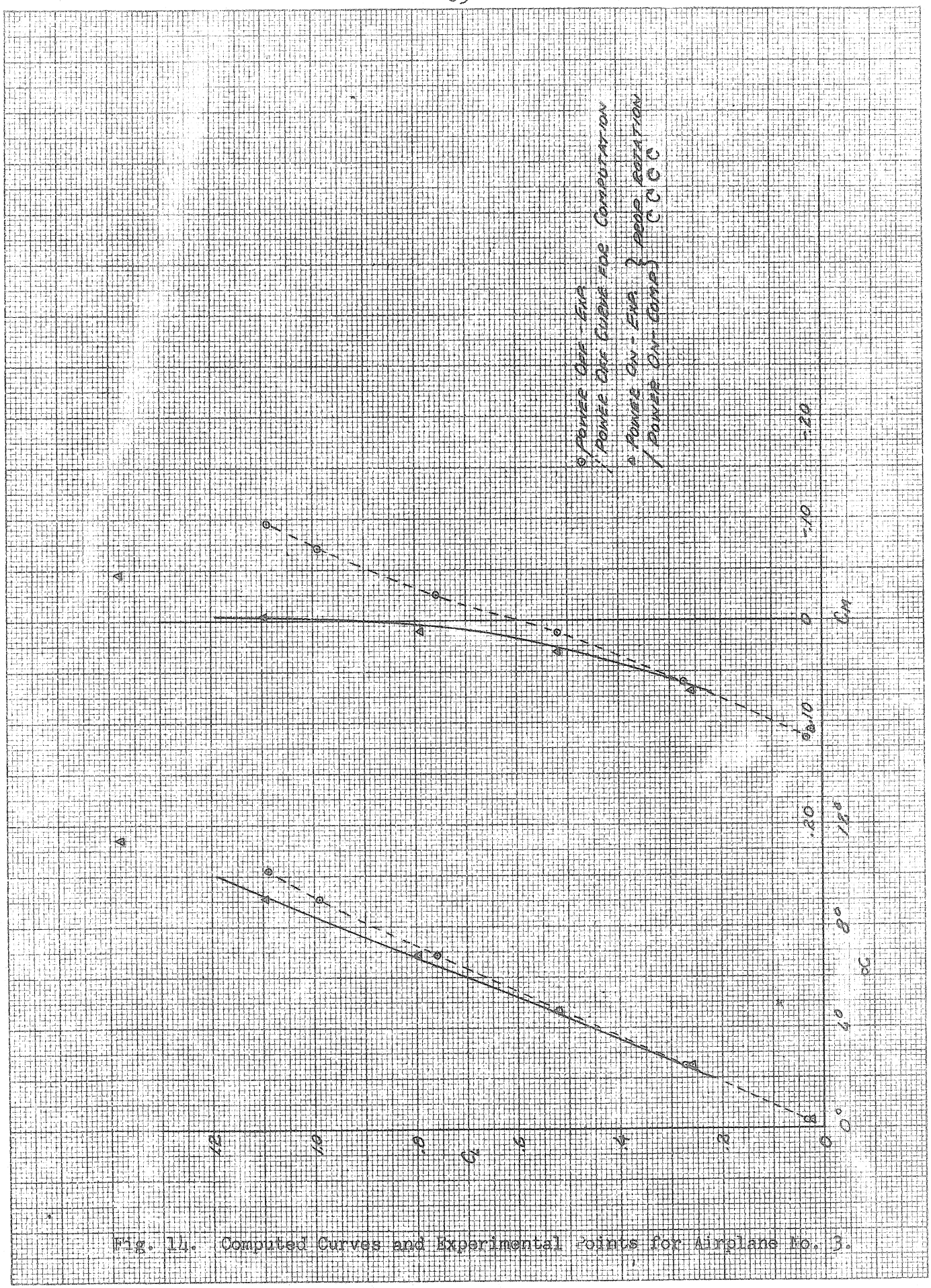

Fig. 14. Computed Curves and Experimental Points for Airplane No. 3.

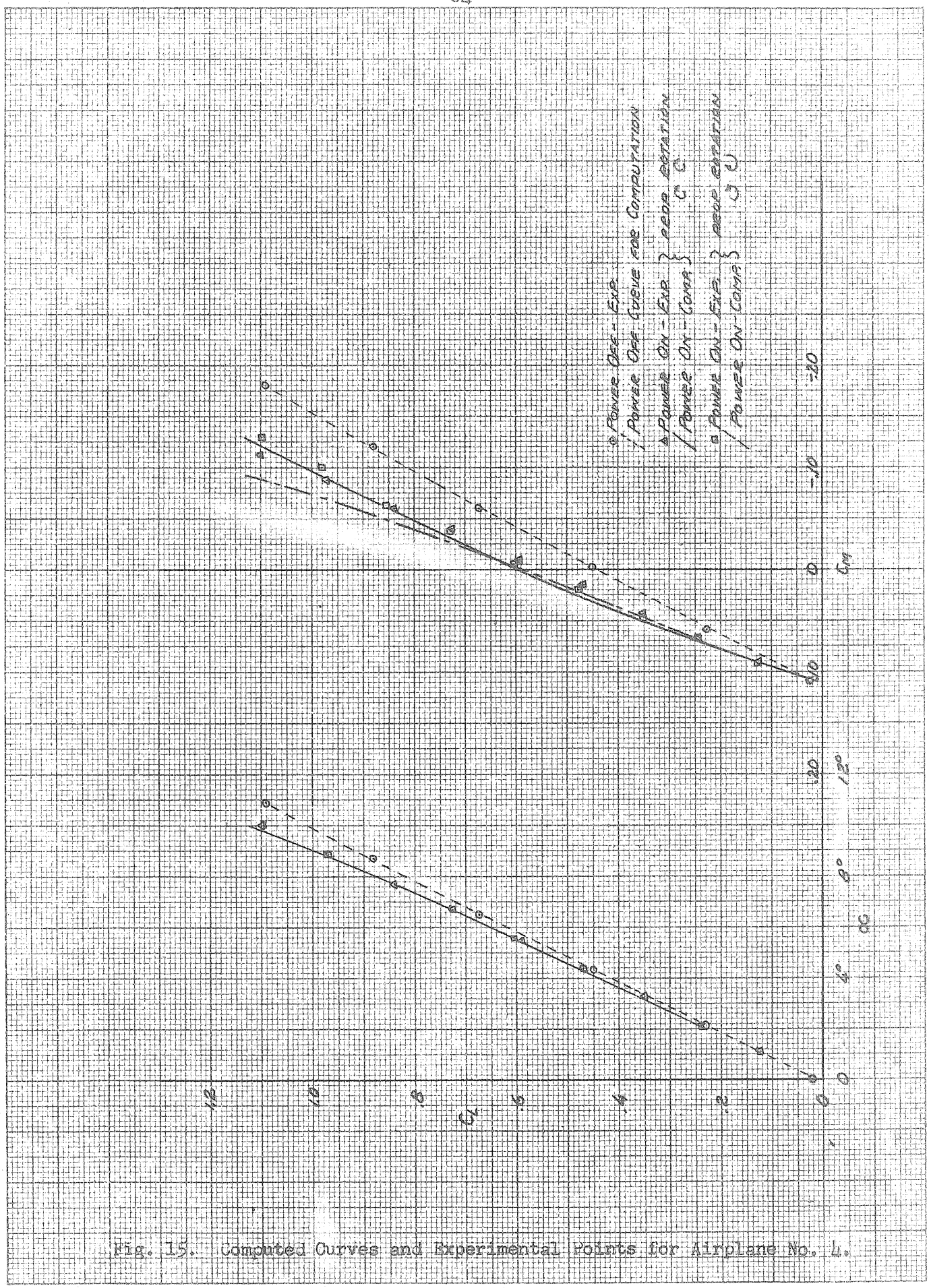

Fig. 15. Computed Curves and Experimental Points for Airplane No. 4.

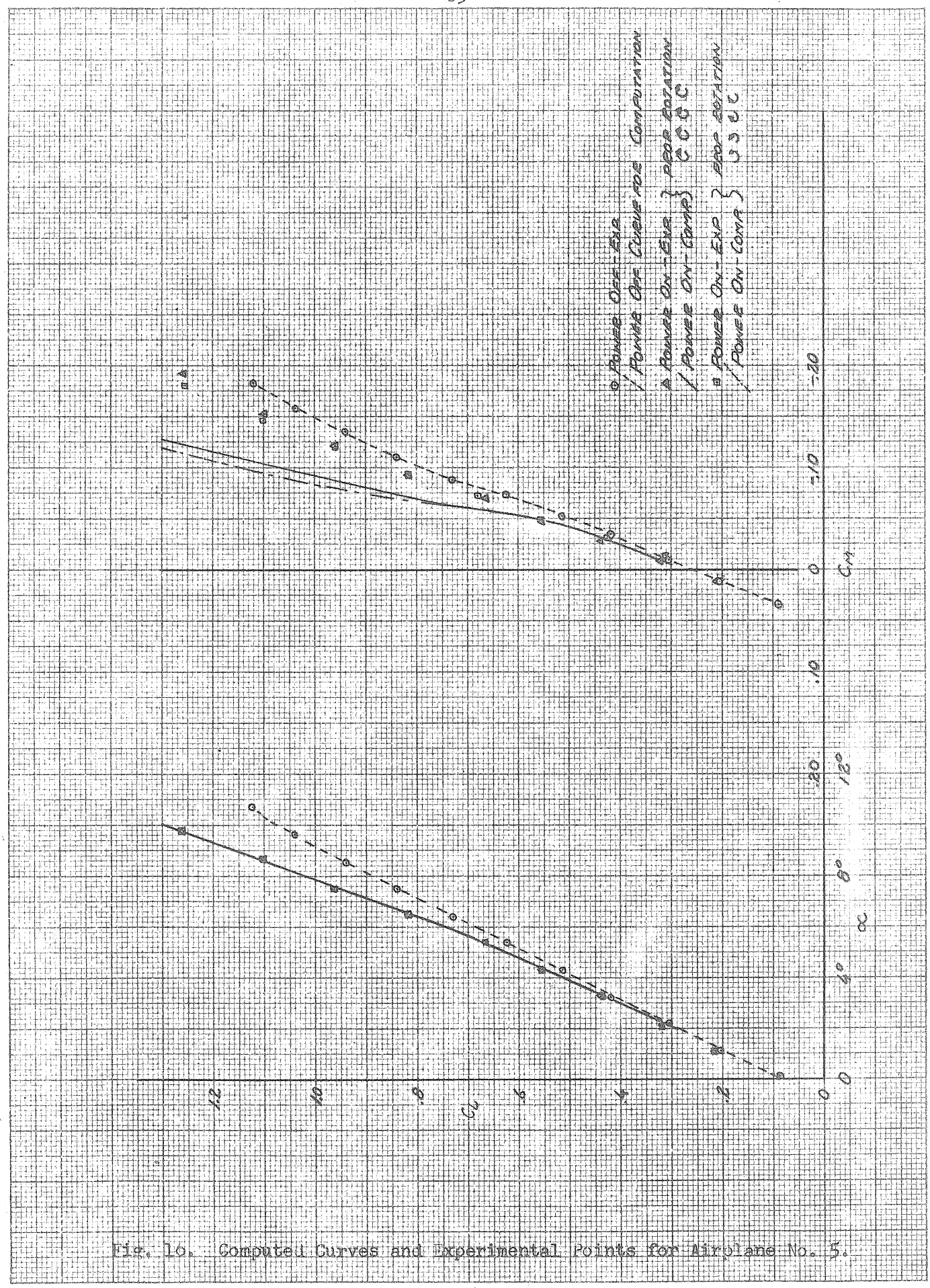

Fig. 10. Computed Curves and Experimental Points for Airplane No. 5.

Quantity	No.	How Formed	Airplane #1	Airplane #2	Airplane #3
c	1		.896	.927	.844
D	2		1.12	1.22	.958
A_p	3		1.04	.71	i=1,4: .583 / i=2,3: .666
A_p/c	4	3 / 1	1.16	.77	i=1,4: .690 / i=2,3: .790
a_o	5		5.65	5.65	5.65
a_t	6		3.73	3.73	3.50
B_p	7		-.032	-.030	i=1,4: .076 / i=2,3: .028
B_p/c	8	7 / 1	-.036	-.032	i=1,4: .090 / i=2,3: .034
b	9		.12	.12	.074
n	10		4	4	3
Q	11	9 10 / 0.7π 2	.195	.179	.105
ϵ	12		2	2	4
ϵk	13		0	0	0
i_p	14		0	-.0873	-.0524
i_t	15		-.0524	-.1245	-.0305
J	16		.99	.99	.96
S	17		6.89	7.22	7.27
S_t	18		1.95	1.68	2.03
x_p	19		-1.04	-.71	-.666
x_t	20		3.53	4.08	3.87
x_w	21		0	0	0
y_p	22		-.032	-.080	0
y_t	23		.534	.800	.600
y_w	24		-.030	.210	.145
z_p	25		1.14	1.20	.923

Fig. 17. Series O Calculations for Airplanes No. 1, 2, and 3.

Quantity	No.	How Formed	Airplane #1	Airplane #2	Airplane #3
z_t	26		1.63	1.61	1.54
η_t	27		.75	.80	.80
θ_p	28		0	0	0
$(y_t - y_p)/D$	29	23 - 22 / 2	.554	.722	.626
$(x_t - x_w)/D$	30	20 - 21 / 2	3.15	3.34	2.71
$(x_t - x_p)/D$	31	20 - 19 / 2	4.07	3.92	4.74
$(z_p - z_t)/D$	32	25 - 26 / 2	-.435	-.335	-.637
$1 + \frac{x_w - x_p}{\sqrt{D^2/4 + (x_w - x_p)^2}}$	33		1.88	1.76	1.81
$E\sqrt{D/S}$	34	12 16 2 / 17	.322	.335	.511
$D/2z_t$	35	21 / 2 26	.343	.378	.312
$a_t \eta_t \frac{S_A}{S} \frac{x_t}{c}$	36	6 27 18 20 / 17 17	3.10	3.06	3.58
D^2/S	37	2^2 / 17	.182	.206	.126
Prop. Blade Type	38		II	II	I
Stabilizer Taper Ratio	39		3	3	2

Fig. 17. (Contd) Series O Calculations for Airplanes No. 1, 2, and 3.

Quantity	α	C_{L_o}	C_L	T_C	J	J^2	C_T	T_C'	ET_C'
Number	101	102	103	104	105	106	107	108	109
How Formed						105 ^{2}	104 106	2 104 37	108 12
	2° .035	.09	.09	.011	1.26	1.59	.018	.004	.008
	4° .070	.30	.32	.047	1.14	1.30	.061	.017	.034
	6° .105	.51	.55	.096	1.03	1.06	.099	.035	.070
	8° .140	.71	.79	.157	.93	.87	.136	.057	.114
	10° .175	.89	1.01	.212	.85	.72	.153	.078	.156

A	B	AQ	$BC_T/10$	$AQ + BC_T/10$	R	C	F	$\alpha + i_p$	e_v
110	111	112	113	114	115	116	117	118	119
Fig. 2	Fig. 2	110 11	111 107 /10	112 + 113	114 37	114/2	Fig. 3	101 + 14	117 118
1.20	1.55	.234	.003	.237	.0432	.118	.14	.035	.005
1.15	1.62	.224	.010	.234	.0426	.117	.17	.070	.012
1.05	1.74	.205	.017	.222	.0404	.111	.21	.105	.0221
1.01	1.80	.197	.024	.221	.0402	.110	.24	.140	.034
.94	1.96	.183	.030	.213	.0388	.107	.27	.175	.047

Fig. 18. Series I Calculations for Airplane No. 1.

QUATITY	$8T_c/\pi$	$1+\frac{8T_c}{\pi}$	$\sqrt{1+\frac{8T_c}{\pi}}$	$-1+\sqrt{1+\frac{8T_c}{\pi}}$	u	s	$.6a_0e_v$	$C_{l_0}-.6a_0e_v$	EJ^{DS}/S
NUMBER	[120]	[121]	[122]	[123]	[124]	[125]	[126]	[127]	[128]
HOW FORMED	2.55 [104]	1 + [120]	$\sqrt{[121]}$	[122] - 1	[123]/2	[124] [33]	.6 [5] [119]	[102] - [126]	[34] [125]
	.028	1.028	1.014	.014	.007	.013	.017	.07	.004
	.120	1.120	1.059	.059	.029	.054	.040	.26	.017
	.245	1.245	1.117	.117	.058	.109	.075	.43	.035
	.400	1.400	1.182	.182	.091	.171	.104	.61	.055
	.541	1.541	1.241	.241	.120	.225	.160	.73	.072

ΔC_L	$ET_c'(\alpha+i_p)$	$ER(\alpha+i_p)$	C_L						
[129]	[130]	[131]	[132]						
[128] [127]	[109] [118]	[115] [12] [118]	[102] + [129] + [130] + [131]						
0	0	.003	.09						
.005	.003	.006	.31						
.015	.007	.009	.54						
.034	.016	.011	.77						
.053	.027	.014	.99						

Fig. 18. (Contd) Series I Calculations for Airplane No. 1.

Quantity	α	C_{M_0}	w	$.75kC_L$	$\frac{(x_a-x_w)(.75kC_L)}{D}$	$.75\epsilon_v$	$\alpha-.75\epsilon_v$	$\frac{(x_a-x_h)(\alpha-.75\epsilon_v)}{D}$	v
Number		201	202	203	204	205	206	207	208
How formed				.75 k 132	203 30	.75 119	101 - 205	206 31	204 - 207
	2°	-.095	.032	.002	.006	.004	.031	.126	.434
	4°	-.065	.040	.007	.022	.009	.061	.248	.328
	6°	-.032	.047	.013	.041	.017	.082	.333	.263
	8°	0	.054	.018	.057	.025	.115	.467	.144
	10°	.030	.058	.023	.072	.035	.140	.568	.058

$F\theta_p$	h	U	$DU/2z_t$	G	$8GT_c/\pi$	$1+\frac{8GT_c}{\pi}$	$1.2\epsilon_v(1+\frac{8GT_c}{\pi})$	$\alpha+i_t$	$\alpha+i_t+k\epsilon-w$
209	210	211	212	213	214	215	216	217	218
117 28	32 - 209	Fig.	211 35	Fig.	213 120	1 + 214	1.2 119 213 21	101 + 18	217 + 13 - 202
0	-.435	.1	.03	.02	0	1	0	-.017	-.049
0	"	1.3	.45	.32	.038	1.038	.005	.018	-.022
0		1.7	.58	.47	.115	1.115	.016	.053	.006
0	↓	2.2	.75	.65	.260	1.260	.037	.088	.034
0	-.435	2.4	.82	.72	.402	1.402	.063	.123	.065

Fig. 19. Series II Calculations for Airplane No. 1.

QUANTITY	$\frac{(\alpha+i_t+\kappa e-w)}{(1+8GTc/\pi)}$		$\frac{-C_{N_t} S_t x_t}{SC}$	$-ET_c' B_p/C$	$\frac{ER(\alpha+i_p)A_p}{C}$	C_M
NUMBER	[219]	[220]	[221]	[222]	[223]	[224]
HOW FORMED	[215] [218]	[219] - [216]	-[220] [36]	[109] [8]	[131] [4]	[201] + [221] + [222] + [223]
	-.049	-.049	.154	0	.003	.062
	-.023	-.028	.086	.001	.007	.029
	.007	-.009	.030	.003	.010	.011
	.043	.006	-.021	.004	.013	-.004
	.091	.028	-.086	.066	.016	-.034

Fig. 19 (Contd) Series II Calculations for Airplane No. 1.